DEFENCE
SCIENCE & TECHNOLOGY

Sep 2002

DSTO

Mode-partition Noise in Semiconductor Lasers

Linh V.T. Nguyen

DSTO-RR-0244

221 149

DEFENCE
SCIENCE & TECHNOLOGY

Mode-partition Noise in Semiconductor Lasers

Linh V. T. Nguyen

Electronic Warfare and Radar Division
Systems Sciences Laboratory

DSTO-RR-0244

ABSTRACT

The primary goal of this research activity is to understand the range of applicability of different types of lasers to a variety of Electronic Warfare (EW) applications. This work helps by providing a detailed understanding of mode-partition noise (MPN) in multi-mode Fabry-Perot (FP) semiconductor lasers. Mode partitioning in semiconductor lasers describes how the intensities of all longitudinal optical modes fluctuate as they compete with each other for a common injected-carrier population.

The results presented in this report include both numerical simulations and experimental measurements. The numerical simulations are based on a noise-driven 21-mode rate-equation laser model, which enables multiple mode partition to be modelled. The formulation of the laser model allows for variation of laser parameters to investigate their effect on mode-partition noise. To the author's best knowledge, only studies with variations of trivial laser parameters have been reported previously. The results in this report go beyond these existing studies in the literature.

Experimental measurements are used to verify simulations where possible. The main difficulty in this work is having laser devices with different parameters as in the simulations. In addition, the available laser device operates in different regimes as a function of injected current, making it difficult to extract parameters with good certainty to simulate the device.

RELEASE LIMITATION

Approved for Public Release

Published by

DSTO Systems Sciences Laboratory
PO Box 1500
Edinburgh South Australia 5111 Australia

Telephone: (08) 8259 5555
Fax: (08) 8259 6567

AR-012-452
September 2002

APPROVED FOR PUBLIC RELEASE

Mode-partition Noise in Semiconductor Lasers

Executive Summary

Mode partitioning in semiconductor lasers describes how the intensities of all longitudinal optical modes fluctuate. In the past, investigations into mode-partition noise (MPN) in semiconductor lasers have been driven mainly by applications in telecommunications. In this report, MPN in semiconductor lasers is numerically and experimentally investigated. The investigation is focused on multi-mode Fabry-Perot (FP) semiconductor lasers and their applicability to microwave photonic signal processing in Electronic Warfare (EW) systems. FP laser devices are useful in microwave photonic signal processing because of their incoherent properties in comparison to single-mode distributed feedback (DFB) devices.

It is numerically determined that the mode partition in multi-mode semiconductor lasers depends strongly on the dynamics of relaxation oscillation and hence self-saturation, or gain compression, of the longitudinal optical modes. Self-saturation dampens relaxation-oscillation producing a Gaussian modal power probability distribution; compared to a quasi-uniform power probability distribution when no self-saturation was simulated.

Experimentally, it was extremely difficult (if not impossible) to find various multi-mode semiconductor lasers with different self-saturation values to compare with simulations. Using a high-power Fabry-Perot laser module, noise power probability distributions were measured and found to be Gaussian. This observation was supported by the highly damped nature of the relative-intensity noise-spectrum of the total optical output of the laser device.

The overall finding presented in this report highlights the influence of self-saturation on mode partitioning in FP semiconductor lasers. In FP laser devices, strong self-saturation produces MPN whose probability distributions are Gaussian, similar to intensity noise distributions from DFB devices. This finding suggests that multi-mode laser devices with a high level of self-saturation can be used as multi-wavelength sources in microwave photonic signal processing for EW applications, in which wavelength-division multiplexing techniques based on fibre Bragg gratings are employed, without experiencing any unnecessary system performance penalty due to MPN.

Author

Linh V. T. Nguyen
Electronic Warfare & Radar Division

Linh Nguyen received a Bachelor of Science and Electrical & Electronic Engineering from the University of Adelaide in 1992 and 1993, respectively. On the completion of his undergraduate studies, he was awarded an Australian Postgraduate Research Award to undertake postgraduate study at the Photonics Research Laboratory, Australian Photonics Cooperative Research Centre, Department of Electrical & Electronic Engineering, University of Melbourne. His research thesis was on numerical modelling of spectral properties and ultra-fast dynamics in semiconductor lasers using the Transmission-Line Laser Modelling technique. He graduated with a degree of Doctor of Philosophy from the University of Melbourne in 1997.

After submitting his thesis, he started working at the Photonics Research Laboratory as the Laboratory Manager. After 12 months, he went on to work for Vicom Australia Pty. Limited (a distributor of telecommunications test and measurement equipment) as a Sales Engineer. This experience then led him to Acterna Asia-Pacific Pty. Limited (former Wavetek Wandel Goltermann Pty. Limited) as a Technical Specialist in telecommunications. During this period, he also managed to complete a Master of Marketing on a part-time basis at the Melbourne Business School.

Currently, Linh Nguyen holds a Research Scientist position in the Electronic Warfare & Radar Division, DSTO Edinburgh, where his research interests are in the field of microwave photonic signal processing and its applications to Electronic Warfare. He is the Task Manager for Photonic Systems Technology in the Electronic Warfare & Radar Division. He actively participates in Opto-Electronics (OE) Hub activities, where he is the Deputy Leader of the OE Hub Advanced Materials & Devices Focus Area.

Contents

1. Introduction

Dense wavelength-division multiplexing (DWDM) techniques are employed in microwave photonic signal processing to increase system design flexibility. Multi-mode Fabry-Perot semiconductor lasers are useful in microwave photonic signal processing because of their incoherent properties in comparison to single-mode distributed feedback (DFB) devices. When FP laser devices are used in DWDM microwave photonic signal processors, various wavelengths would be filtered out and delayed accordingly. It is therefore necessary to understand the intensity fluctuation of each individual longitudinal mode because of the following effects:

1. Each filtered output may not necessarily have the correct power probability distribution, e.g. Gaussian, which is required to represent the statistical nature of the target cross-section in Electronic Warfare (EW) receivers.
2. The relative intensity noise (RIN) of the filtered output is enhanced at low frequencies. This increase in RIN may coincide with microwave frequencies of interest and hence degrade system performance.

Modal intensities in FP semiconductor lasers fluctuate as they compete with each other for a common injected-carrier population. This phenomenon is known as mode partitioning resulting in mode-partition noise (MPN). Naturally, MPN is greatest when there are multiple longitudinal modes with similar modal photon population. It has long been established that photon fluctuation caused by mode partitioning in semiconductor lasers degrades optical system performance. There were many studies in the 1980s to demonstrate how mode-partition noise in nearly single-mode semiconductor lasers can affect the performance of optical communication systems. Examples are listed as References [1]-[6].

The advent and availability of single-mode distributed-feedback (DFB) semiconductor lasers with side-mode suppression ratios greater than 40 dB caused a drop in the interest in studying MPN, as these single-mode laser devices have superior transmission performance for telecommunications. Studies on mode partition have been few and far between in the 1990s [7,8]. It can be said that the 1980s were device-focused, while research in the 1990s tended to be more system-related. From the point of view of device-focused understanding of mode partition in semiconductor lasers, Liu *et al.* [1] have been most accomplished in providing statistical measurements while Marcuse [9]-[12] stood out with computer simulations of photon fluctuations based on noise-driven rate equations.

In general, single-mode DFB semiconductor lasers have Gaussian power probability distributions. Similarly, it is understood and accepted, that the total output power of a multi-mode Fabry-Perot (FP) semiconductor laser has a Gaussian power probability distribution due to the Central Limit Theorem. In addition, it is accepted that each longitudinal mode fluctuates more compared to the total output because of mode

partitioning [13]. However, it is not well understood how mode partitioning and modal power probability distributions behave as a function of various laser parameters such as self- and cross-saturation.

The interest in mode partitioning in multi-mode FP semiconductor lasers within the Electro-Optic Technology Group, Electronic Warfare & Radar Division, relates to microwave photonic signal processing. In particular, the interest lies in the utilisation of FP lasers as cheap and compact multi-wavelength sources in the application of DWDM to microwave photonic signal processing [14]-[16].

In this report, computer simulation of photon fluctuations using single-mode and multi-mode rate-equation laser models are presented to gain an understanding of how mode partitioning and modal power probability distributions behave as a function of various laser parameters such as self- and cross-saturation. The structure of this report is arranged into following sections:

- *Semiconductor Laser Rate-Equation Models* section provides details of both single-mode and multi-mode laser models, and device parameters, to be used in the numerical simulations.
- The simulation results are then presented in *Modelling Results*. In particular, mode partitioning and modal power probability distributions as a function of various laser parameters will be presented.
- *Experimental Investigation* section explores a series of intensity noise measurements from a high-power FP semiconductor laser module.
- *Conclusions* summarise the findings of this report.
- *Recommendations* detail the application of FP laser devices in microwave photonic signal processing and future research directions.

2. Semiconductor Laser Rate-Equation Model

The numerical modelling presented in this report is based on rate equations describing the interaction between carrier density (N) and photon number (S) in the active region of a semiconductor laser diode. In particular, the rate-equation laser models used are based on the works of Ogita *et al.* [8] and Marcuse [9]-[12].

2.1 Deterministic Rate Equations

2.1.1 Single-Mode Model

The single-mode rate-equation model is represented as below:

$$\frac{dS}{dt} = g(N,S)S - \frac{S}{\tau_{ph}} + \Gamma\beta V_{act} B_{eff} N^2 \tag{1}$$

$$\frac{dN}{dt} = \frac{I(t)}{qV_{act}} - \frac{g(N,S)S}{V_{act}} - B_{eff} N^2 \tag{2}$$

$$g(N,S) = \Gamma a(N - N_o) - B_c(N - N_s)S \tag{3}$$

Equation 1 represents the rate of change in photon number in the active region, which includes contributions from stimulated and spontaneous emissions minus those emitted through the facets and lost in the waveguide of the active region. Equation 2 represents the rate of change in carrier density, which includes injected carriers minus those being converted to photons by stimulated and spontaneous emissions. Equation 3 is the optical gain experienced by a photon propagating through the active region.

The definition for photon lifetime is:

$$\frac{1}{\tau_{ph}} = \frac{c}{n_g}\left(\alpha_{\text{int}} + \frac{1}{2L}\ln\frac{1}{R_1 R_2}\right) \tag{4}$$

Definitions and typical values of various laser parameters are from Ogita *et al.* [8]:

Table 1: Laser parameters as extracted from Ogita et al. [8].

Name	Symbol	Value	Unit
Optical confinement factor	Γ	0.25	
Differential gain	a	1.62×10^{-12}	m^3/s
Transparency carrier density	N_o	1.2×10^{24}	m^{-3}
Nonlinear gain transparency carrier density	N_s	1×10^{24}	m^{-3}
Spontaneous emission	β	5×10^{-5}	
Effective recombination rate	B_{eff}	3×10^{-16}	m^3/s
Cavity length	L	300×10^{-6}	m
Cavity volume	V_{act}	6.75×10^{-17}	m^3
Group index	n_g	3.7	
Facet reflectivity	R_1, R_2	0.32	
Internal loss	α_{int}	1000	m^{-1}
Self-saturation factor	B_c	2×10^{-20}	m^3/s
Electronic charge	q	1.602×10^{-19}	C
Speed of light in vacuum	c	3×10^{8}	m/s
Injected current	$I(t)$	$0.015 \rightarrow 0.030$	A

The single-mode rate-equation laser model is suitable to simulate single-mode DFB lasers or nearly single-mode FP lasers, but it is not suitable for model multi-mode FP laser diodes with spectral dependence and especially when mode partitioning is under investigation.

2.1.2 Multi-Mode Model

Ogita *et al.* [8] demonstrated that simulation of 21 longitudinal optical modes are sufficient to model multi-mode FP laser diodes. Hence, the multi-mode modelling presented here will be based on the same model [8] so that results can be crosschecked:

$$\frac{dS_p}{dt} = g_p(N,S_1\ldots S_{21})S_p - \frac{S_p}{\tau_{ph}} + \Gamma\beta V_{act}B_{eff}N^2 \tag{5}$$

$$\frac{dN}{dt} = \frac{I(t)}{qV_{act}} - \sum_{p=1}^{21}\frac{g_p(N,S_1\ldots S_{21})S_p}{V_{act}} - B_{eff}N^2 \tag{6}$$

$$g_p(N,S_1\ldots S_{21}) = A_p - B_pS_p - \sum_{q\neq p}(D_{p,q}+H_{p,q})S_q \tag{7}$$

$$A_p = \Gamma a\left(N - N_o - b\left(\lambda[p] - \left[\lambda_{peak}(N) + \Delta\lambda_{gp}\right]^2\right)\right) \tag{8}$$

$$B_p = B_c(N - N_s) \tag{9}$$

$$D_{p,q} = \frac{4}{3} B_p \frac{1}{1+(\omega_p - \omega_q)^2 \tau_{in}^2} \tag{10}$$

$$H_{p,q} = H_c(N - N_o)\frac{1}{\omega_p - \omega_q} \tag{11}$$

$$\lambda_{peak}(N) = \lambda_c - \left(\frac{\Delta\lambda_{peak}}{\Delta N}\right)N \tag{12}$$

$$\lambda[11] = \lambda_{peak}\left(N_o + \frac{1}{\tau_p \Gamma a}\right) \tag{13}$$

Equation 5 represents the rate of change in photon number of each longitudinal mode, while Equation 6 represents the rate of change in carrier density in a common pool being competed for by all 21 longitudinal optical modes. The optical gain shown in Equation 7 is more complicated than for single-mode model. The multi-mode optical gain now consists of the following:

1. Linear gain with parabolic spectral dependence near the gain peak, Equation 8. A new parameter, $\Delta\lambda_{gp}$, is introduced to allow for a shift in the gain peak.
2. Self-saturation or gain compression, Equation 9.
3. Symmetric cross-saturation caused by spectral-hole burning [8]; i.e. the mode with the largest photon population would capture the majority of the available carriers, Equation 10. This term suppresses all the side modes making the laser single-moded, and so its mode-partition noise is not interesting to investigate.
4. Asymmetric cross-saturation caused by modal intermodulation due to the carrier dependence of refractive index in the active region, i.e. the linewidth enhancement factor [8,17]. The intermodulation described here is similar to that in four-wave mixing in semiconductor optical amplifiers. This term is generally referred to as asymmetric nonlinear gain (ANG). Its effect is a transfer of modal power from low to long wavelengths.

The modelled optical spectrum of the multi-mode FP laser diode is centred at mode 11 with peak wavelength at threshold carrier density, as described by Equations 12 and 13. The majority of the parameters are as defined for the single-mode model, with additional definitions and typical values as follow [8]:

Table 2: Additional laser parameters for multi-mode rate equations as used by Ogita et al. *[8].*

Name	Symbol	Value	Unit
Centre wavelength at zero carrier density	λ_c	1360	nm
Laser mode spacing	$\Delta\lambda_m$	0.8	nm
Gain broadening factor	b	9×10^{20}	$m^{-3}nm^{-2}$
Peak-gain wavelength shift	$\frac{\Delta\lambda_{peak}}{\Delta N}$	2.7×10^{-23}	m^3nm
Intraband relaxation time	τ_{in}	1×10^{-13}	s
Asymmetric nonlinear gain factor	H_c	8×10^{-9}	m^3/s^2

The mode spacing is determined by the cavity length and refractive index. It is used to define the wavelengths of all longitudinal optical modes, $\lambda[p]$, relative to the centre of the optical spectrum, which is defined by the threshold condition in Equation 13.

2.2 Noise-Driven Rate Equations

2.2.1 Single-Mode Model

Noise-driven rate equations have similar form to the deterministic models. There would be additional random noise functions driving both the photon number and carrier density equations. The single-mode noise-driven rate-equation model would take the following form:

$$\frac{dS}{dt} = g(N,S)S - \frac{S}{\tau_{ph}} + \Gamma\beta V_{act}B_{eff}N^2 + F_S(t) \tag{14}$$

$$\frac{dN}{dt} = \frac{I(t)}{qV_{act}} - \frac{g(N,S)S}{V_{act}} - B_{eff}N^2 + F_N(t) \tag{15}$$

where $F_S(t)$ and $F_N(t)$ are the random noise functions driving the photon number and carrier density equations, respectively. These noise functions are assumed to be Gaussian [9]. Following the work by Marcuse [9], the stochastic noise functions can be defined in the following forms in any particular time-step, Δt, in the numerical integration algorithm:

$$F_N = \frac{\sigma_N}{\Delta t}x_N \tag{16}$$

$$F_S = r_S\frac{\sigma_S}{\sigma_N}F_N + \frac{\sigma_S}{\Delta t}\sqrt{1-r_S^2}\,x_S \tag{17}$$

$$\sigma_N^2 = \frac{I}{qV_{act}} + \frac{g^+(N,S)S}{V_{act}} + B_{eff}N^2 \tag{18}$$

$$\sigma_S^2 = g^+(N,S)S + \frac{S}{\tau_{ph}} + \Gamma\beta V_{act}B_{eff}N^2 \tag{19}$$

$$r_S = -\frac{g^+(N,S)S + \Gamma\beta V_{act}B_{eff}N^2}{\sigma_N\sigma_S} \tag{20}$$

$$g^+(N,S) = \Gamma a(N+N_o) + B_c(N+N_s)S \tag{21}$$

Equation 18 and 19 are effectively the variances of F_N and F_S, and r_S is the correlation coefficient. Further details can be referred to in Reference 9. Both x_S and x_N are random variables with Gaussian distributions in the interval $0 \le |x| < \infty$. These Gaussian-distributed random variables can be generated easily from a uniform random variable, $0 \le u \le 1$.

$$x = \pm\sqrt{2}\,\mathrm{erf}^{-1}(u) \tag{22}$$

The sign in Equation 22 is randomly chosen, while erf^{-1} is the inverse error function. The uniform random generator function is readily available in most mathematical software packages and computer languages.

2.2.2 Multi-Mode Model

Similar to the single-mode model, the noise-driven 21-mode laser model is:

$$\frac{dS_p}{dt} = g_p(N,S_1\ldots S_{21})S_p - \frac{S_p}{\tau_{ph}} + \Gamma\beta V_{act}B_{eff}N^2 + F_{S_p}(t) \tag{23}$$

$$\frac{dN}{dt} = \frac{I(t)}{qV_{act}} - \sum_{p=1}^{21}\frac{g_p(N,S_1\ldots S_{21})S_p}{V_{act}} - B_{eff}N^2 + F_N(t) \tag{24}$$

The various random noise functions driving the carrier density and the photon number in each longitudinal mode can be determined based on Marcuse [9]:

$$F_N = \frac{\sigma_N}{\Delta t}x_N \tag{25}$$

$$F_{S_p} = r_{S_p}\frac{\sigma_{S_p}}{\sigma_N}F_N + \frac{\sigma_{S_p}}{\Delta t}\sqrt{1-r_{S_p}^2}\,x_{S_p} \tag{26}$$

$$\sigma_N^2 = \frac{I}{qV_{act}} + \sum_{p=1}^{21}\frac{g_p^+(N,S_1\ldots S_{21})S_p}{V_{act}} + B_{eff}N^2 \tag{27}$$

$$\sigma_{S_p}^2 = g_p^+(N,S_1 \ldots S_{21})S_p + \frac{S_p}{\tau_{ph}} + \Gamma\beta V_{act} B_{eff} N^2 \tag{28}$$

$$r_{S_p} = -\frac{g_p^+(N,S_1 \ldots S_{21})S_p + \Gamma\beta V_{act} B_{eff} N^2}{\sigma_N \sigma_{S_p}} \tag{29}$$

$$g_p^+(N,S_1 \ldots S_{21}) = A_p^+ + B_p^+ S_p + \sum_{q \neq p} \left(D_{p,q}^+ + \left| H_{p,q}^+ \right| \right) S_q \tag{30}$$

$$A_p^+ = \Gamma a\left(N + N_o + b\left(\lambda[p] - \lambda_{peak}(N)\right)^2\right) \tag{31}$$

$$B_p^+ = B_c(N + N_s) \tag{32}$$

$$D_{p,q}^+ = \frac{4}{3} B_p^+ \frac{1}{1 + (\omega_p - \omega_q)^2 \tau_{in}^2} \tag{33}$$

$$\left| H_{p,q}^+ \right| = H_c(N + N_o) \frac{1}{|\omega_p - \omega_q|} \tag{34}$$

2.3 Implementation Issues

All of the modelling work presented in this report was implemented in Mathematica. The numerical integration routine is chosen to be the 4th-order Runge-Kutta method, which was used by both Ogita *et al.* [8] and Marcuse [9]-[12]. The routine is available in most good applied mathematics textbooks, e.g. "Advanced Engineering Mathematics" by Kreyzig [18].

The initial conditions for both carrier density and photon number in both single- and multi-mode models are set as below:

$$\begin{aligned} N[0] &= N_o \\ S[0] &= 0 \end{aligned} \tag{35}$$

This is logical because, at the transparency carrier density, there is no optical gain and thereby very few photons. If the carrier density were set to 0, then it would simply take longer. Equation 35 is also therefore a means to reduce the time it takes to perform each simulation.

Laser device parasitic can be modelled by using a time-constant, τ_{RC}, modifying the DC bias current, I_{DC}, when turning the laser model on as follows:

$$I(t) = I_{DC}\left(1 - e^{t/\tau_{RC}}\right) \tag{36}$$

3. Modelling Results

In this section, simulation results from single- and multi-mode deterministic as well as noise-driven laser models are presented to investigate the dependence of mode partition on various laser parameters. The deterministic models were verified with Ogita *et al.* [8].

3.1 Deterministic Single-Mode Results

Using the laser parameters listed in Table 1, the threshold current for the modelled laser diode is 15 mA. Together with a parasitic time-constant of 1 ns, a typical plot of the transient carrier density and photon number from the deterministic single-mode model, Equation 1-3, was simulated with step current of 20 mA. The result is shown in Figure 1 below. It clearly shows the coupled relaxation oscillation that occurs between the carrier density and photon number before reaching steady state. Nonlinear gain and, to a lesser degree, parasitic time-constant can reduce this relaxation oscillation. It is worthwhile to note the timescale over which the steady state is reached in this case, which can be compared to the multi-mode simulation later.

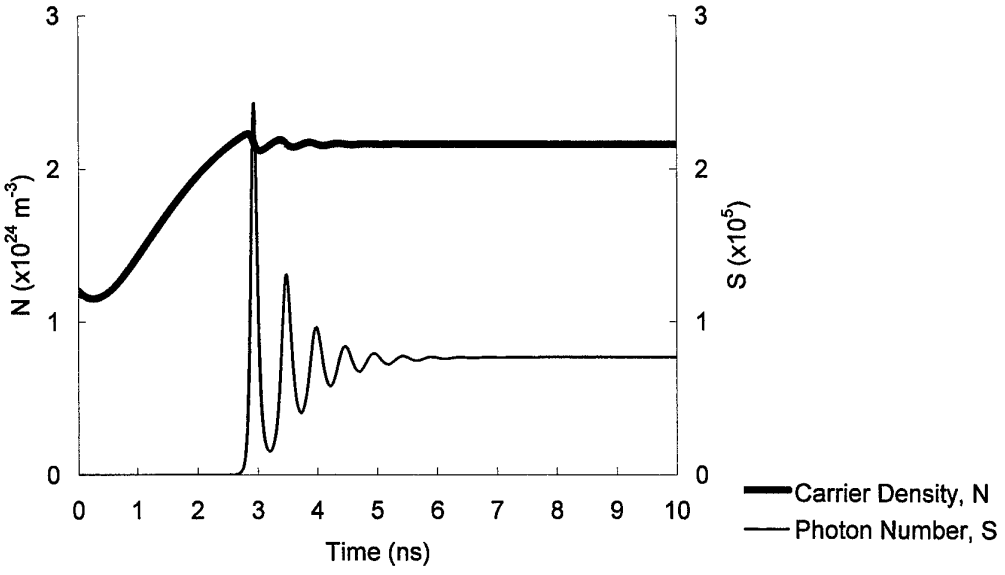

Figure 1: Transient dynamics of carrier density and photon number for a deterministic single-mode rate-equation model with bias current of 20 mA and time-step of 1 ps.

3.2 Noise-Driven Single-Mode Results

The same parameters listed in Table 1 were used in the simulation using the noise-driven single-mode rate-equation model, Equations 14-21. The noise-driven turn-on response of the laser model is plotted in Figure 2.

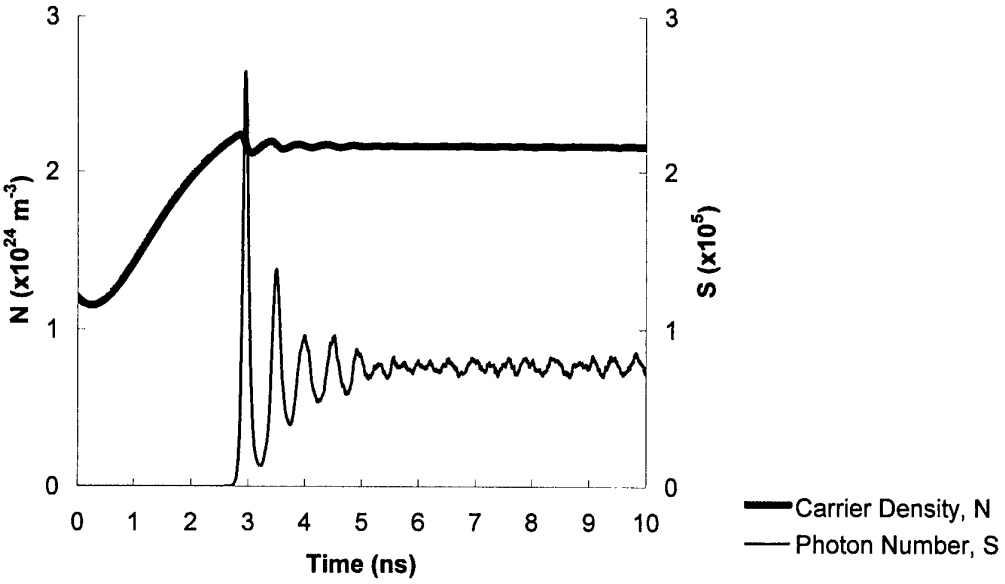

Figure 2: Turn-on dynamics of carrier density and photon number for a noise-driven single-mode rate-equation model with bias current of 20 mA and time-step of 1 ps.

The carrier density responses in Figures 1-2 are similar. The carrier density fluctuation in Figure 2, due to the random driving function in Equation 16, is not significant because of a large steady-state value. The photon number in Figure 2 fluctuates about its average value after the transient relaxation oscillation (between 3 to 6 ns) has ceased. While the fluctuation after the transient relaxation oscillation is random, as modelled by Equations 14-21, the dynamics of relaxation oscillation still govern the behaviour of the fluctuation after 6 ns, as shown in Figure 2. Each random event produces changes in the photon population, but the photon population persists to settle back to its steady state through relaxation oscillation. This is the same principle used by Henry [17] to determine the linewidth enhancement factor.

A plot of the time series as presented in Figure 2 gives very little information concerning its random nature. A more appropriate method is to plot the fluctuation as a probability distribution, i.e. collecting photon-number samples in bins and then dividing the resultant bins by the total number of samples. Three hundred (300) such probability bins were used in the analysis to calculate the probability distribution of the time series. Figures 3-5 illustrate photon number probability distribution as simulated from the noise-driven single-mode laser models.

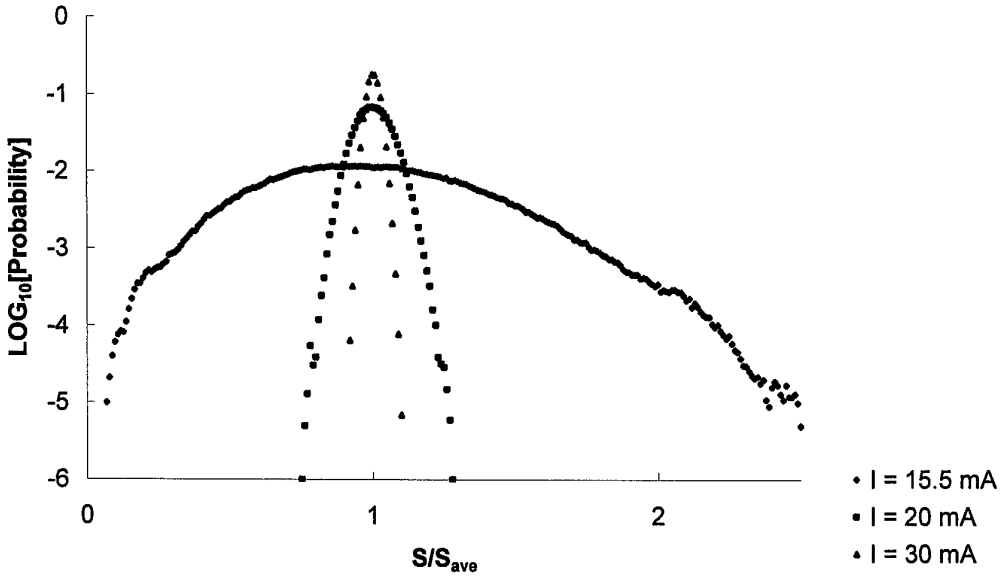

Figure 3: Photon number probability distribution from a noise-driven single-mode model at various bias currents. The data was extracted from simulation using a 1-ps time-step and over a period of 1 μs. The first 10 ns were removed to eliminate the turn-on transient.

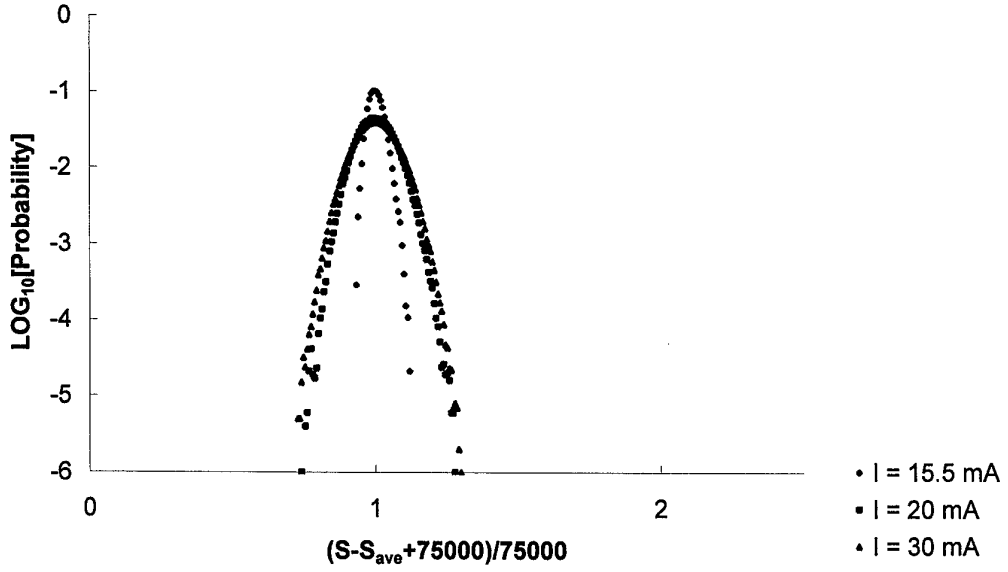

Figure 4: Photon number probability distribution as in Figure 3. The results represent the photon fluctuations with respect to one another. This is achieved by subtracting the average from each photon number series and then normalised to a common average value, i.e. 75,000.

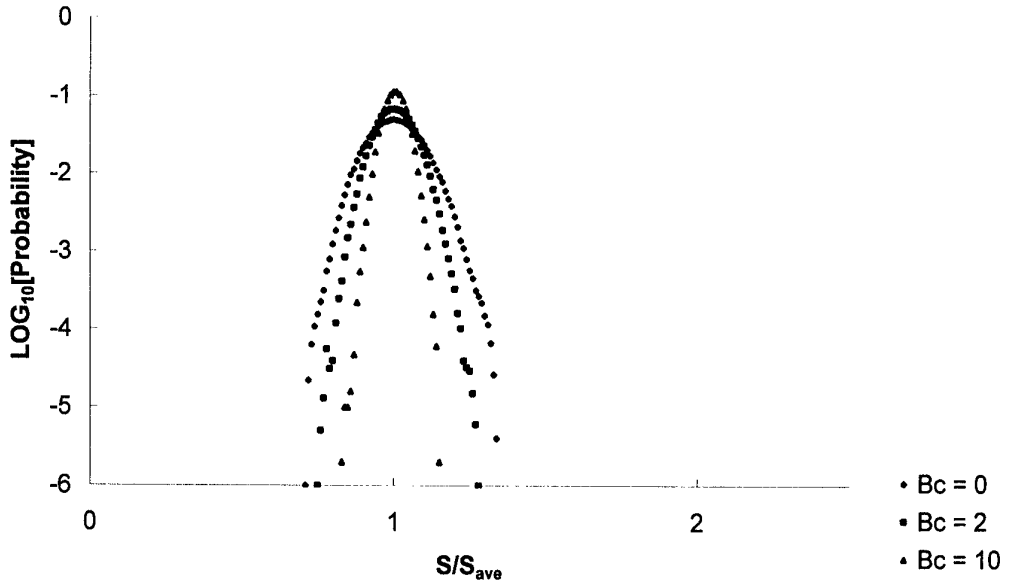

Figure 5: Photon number probability distribution from a noise-driven single-mode rate-equation model with bias current of 20 mA. The data was extracted from simulation using a 1-ps time-step and over a period of 1 μs after the first 10 ns were removed to eliminate the turn-on transient. The magnitudes of self-saturation listed are actually $\times 10^{-20}$ m^3/s. In all three cases, the average photon numbers are the same.

Figure 3 shows a plot of the photon number probability distributions for three bias currents of 15.5 mA, 20 mA and 30 mA. (Note that the threshold current for the laser model is 15 mA.) Just above threshold, it can be seen that the probability distribution deviates from a Gaussian distribution. This can be attributed to the correlation between the carrier density and photon number, as modelled in Equation 20. Marcuse [10] observed a similar result. As the bias current was increased, the probability distribution became more narrow and Gaussian. The narrowing of the probability distribution in Figure 3 is illusionary. As the bias current was increased, the average output photon number also increased. The number of bins used to determine the probability was fixed at 300, which cover a range of photon number from zero to three times the average value. As the average photon number increased with bias current, the normalisation causes the narrowing of the probability distributions.

To take the analysis a step further with the same data presented in Figure 3, the photon number fluctuations with respect to one another was investigated by taking each time series and subtracting its own average value from it. The resultant time series of the fluctuations are then re-normalised to a new common average value, as illustrated in Figure 4. The increase in fluctuations was marginal when the laser was well above threshold, i.e. 20 mA and 30 mA, as shown in Figure 4.

As explained earlier, the dynamics of relaxation oscillation still influence the noise-driven photon number after the transient relaxation oscillation has ceased. Figure 5 shows the photon number probability distribution for three levels of self-saturation at 20 mA. Since the threshold condition for the laser model stays the same for different self-saturation levels, the average photon numbers in all three cases are the same. Figure 5 shows narrowing of the probability distribution for increasing self-saturation level. This is because self-saturation, or gain compression, dampens relaxation oscillation in semiconductor lasers [19].

Changing the differential gain and photon lifetime can also alter the damping, but these parameters also affect the threshold condition of the laser model. Such variation of laser parameters results in different average photon number and thereby changes the width of the probability distribution, as illustrated in Figure 3.

3.3 Deterministic Multi-Mode Results

Deterministic simulations were carried out using Equations 5-9 and 11-13, using parameters listed in Tables 1-2. Equation 10 was not modelled because the single-moded output had already been investigated in section 3.1. The bias current was set to 20 mA, including the parasitic effect. The gain peak was shifted to achieve dual dominant modes to investigate mode partitioning:

Case I: Both self-saturation and asymmetric nonlinear gain were not modelled.
Case II: Self-saturation modelled but not asymmetric nonlinear gain.
Case III: Asymmetric nonlinear gain (ANG) modelled but not self-saturation.
Case IV: Both self-saturation and asymmetric nonlinear gain modelled.

The main reason for simulating dual dominant modes, as shown in Figures 6-9, was to investigate MPN at its strongest level, with the potential to give rise to a uniform distribution between zero and the average total photon number. This is supported by the studies of Marcuse [10]. Single-modedness would only suppress mode partition and give rise to a Gaussian or quasi-Gaussian probability distribution. The optical spectra shown in Figures 6-7 are symmetric, while spectra in Figures 8-9 are asymmetric. Self-saturation is a symmetric property and therefore does not affect the symmetric spectral dependence. The asymmetricity in Figure 8-9 is caused by the intermodulation of the Fabry-Perot modes due to the carrier dependence of refractive index, which is often referred to as ANG.

The transients of the total photon numbers in all four cases are the same and very similar to the transient from the single-mode model in Figure 1. Significant difference arises between single- and multi-mode models when the transients of the total photon numbers are resolved into various modal components, as shown in Figures 6-9. These modal transients can take up to five times longer than the total output to reach steady state as illustrated in Figure 8. Such transfer of modal power is due to the effect of the ANG when simulated on its own.

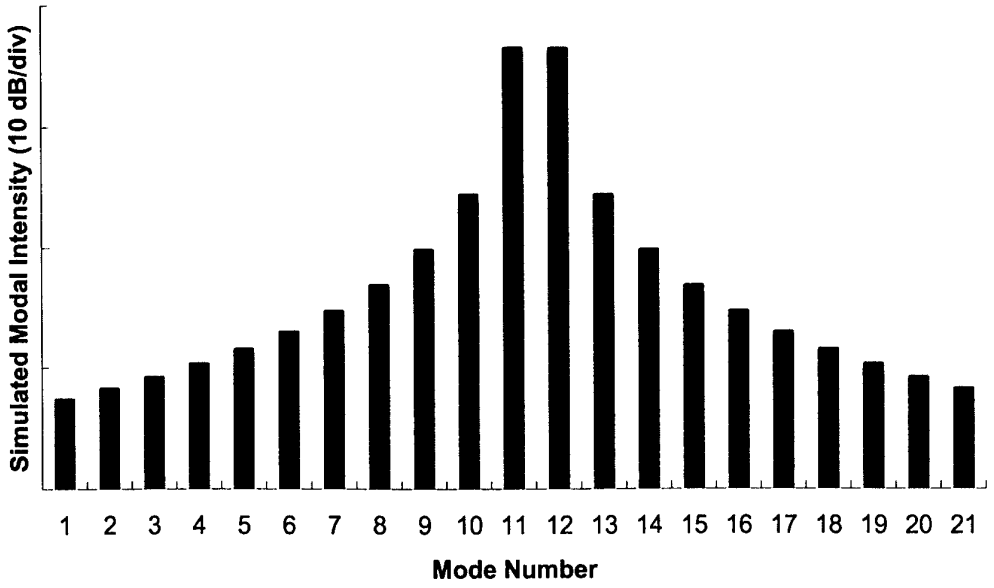

(a) Simulated optical spectrum at steady state.

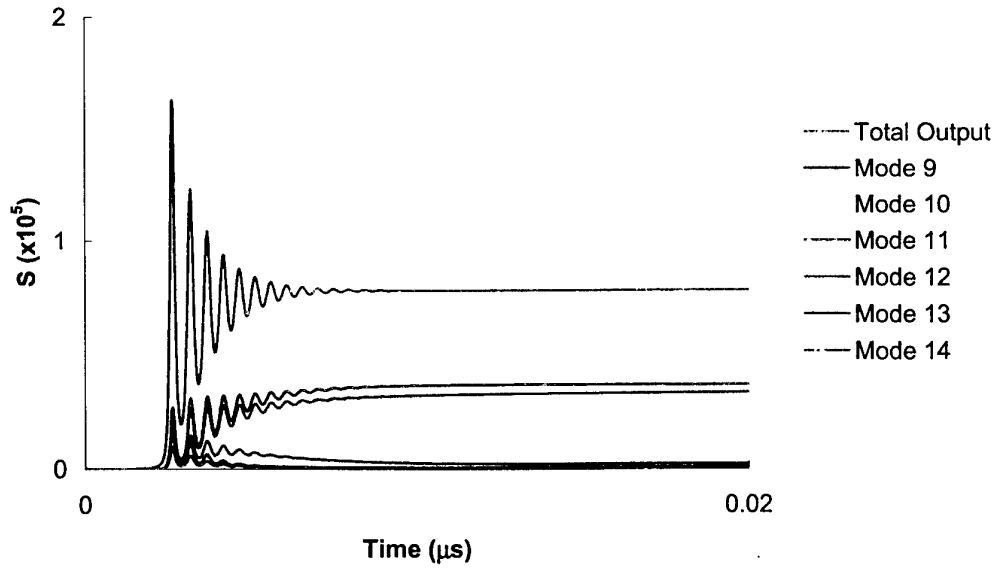

(b) Transient responses of the total output and modes 9-14.

Figure 6: Case I - Multi-mode simulation results biased at 20 mA. The following parameters were used B_c=0, H_c=0 and $\Delta\lambda_{gp}$=+0.418 nm.

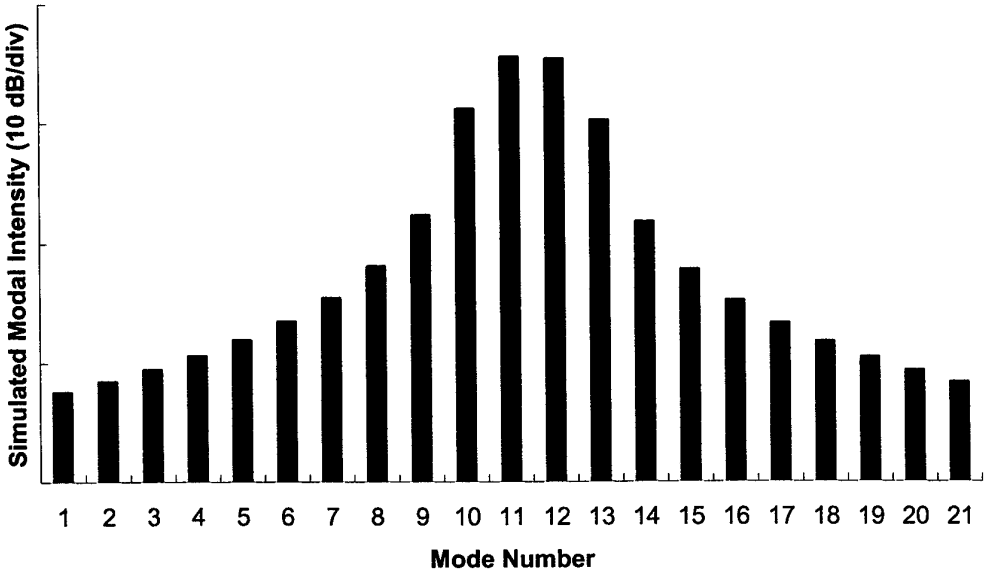

(a) Simulated optical spectrum at steady state.

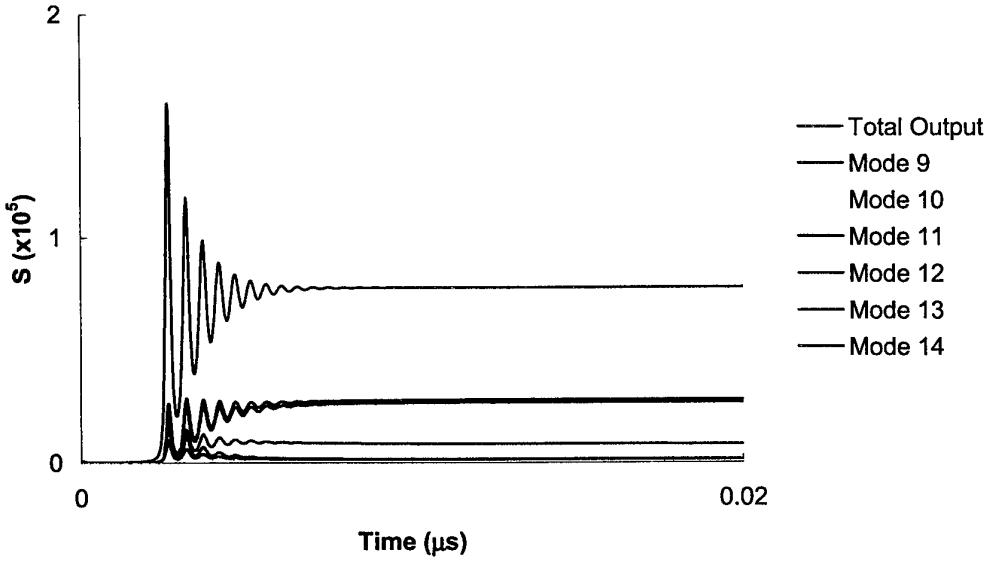

(b) Transient responses of the total output and modes 9-14.

Figure 7: Case II - Multi-mode simulation results biased at 20 mA. The following parameters were used $B_c = 2x10^{-20}\ m^3s^{-1}$, $H_c = 0$ *and* $\Delta\lambda_{gp} = +0.418\ nm$.

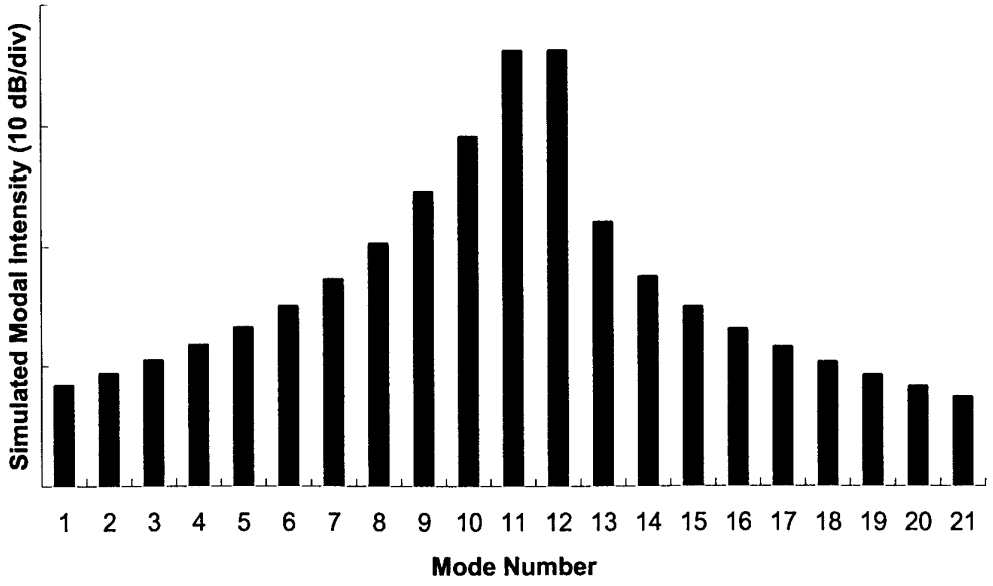

(a) Simulated optical spectrum at steady state.

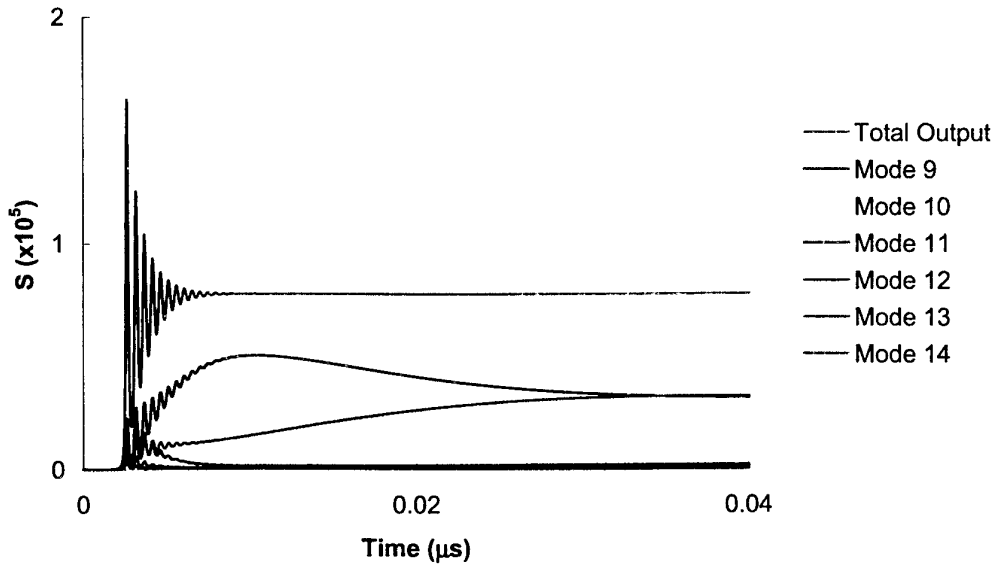

(b) Transient responses of the total output and modes 9-14.

Figure 8: Case III - Multi-mode simulation results biased at 20 mA. The following parameters were used B_c=0, H_c=8x10^{-9} m^{3}s^{-2} and $\Delta\lambda_{gp}$=-0.465 nm.

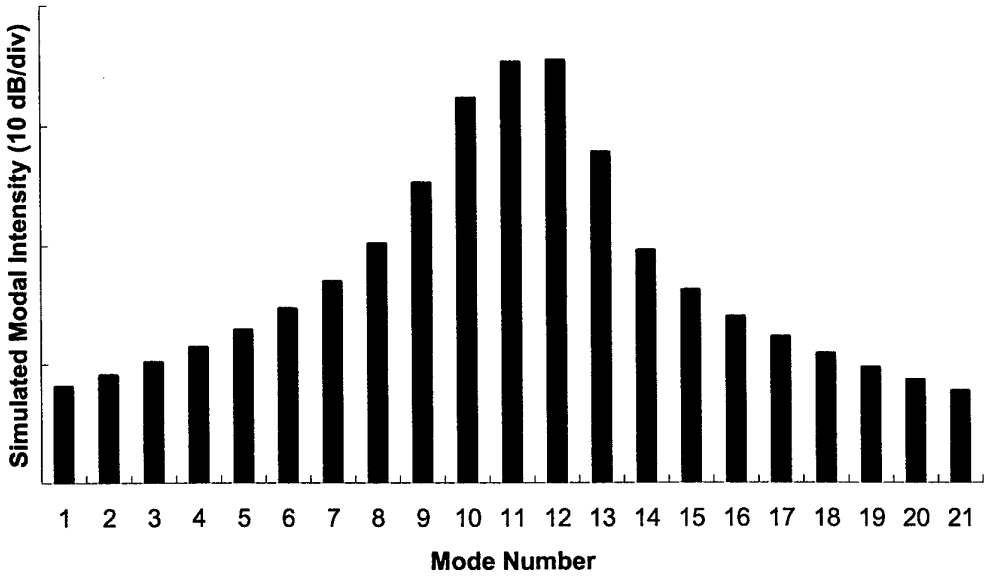

(a) Simulated optical spectrum at steady state.

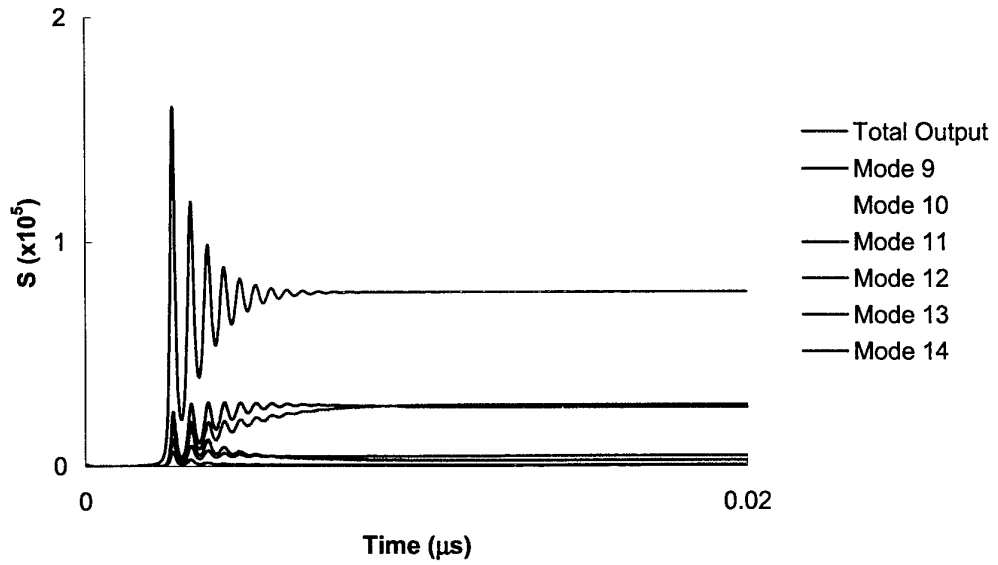

(b) Transient responses of the total output and modes 9-14.

Figure 9: Case IV - Multi-mode simulation results biased at 20 mA. The following parameters were used $B_c = 2 \times 10^{-20}\ m^3 s^{-1}$, $H_c = 8 \times 10^{-9}\ m^3 s^{-2}$ *and* $\Delta\lambda_{gp} = -0.150\ nm$.

3.4 Noise-Driven Multi-Mode Results

Ogita *et al.* [8] took measurements of mode-resolved power transients over a period of up to 200 ns in 1310-nm laser diodes. These measurements suggest a Gaussian probability distribution, as compared to the quasi-uniform distribution statistically measured by Liu *et al.* [1] in 1310-nm laser diodes. The low-bandwidth detector used by Ogita *et al.* [8] would not filter out the low-frequency MPN, which tends to have large magnitude as suggested in the study by Loh [13]. This leads to the explanation that MPN would depend on various laser parameters. Under the investigation to be presented in this section, the aim is to identify which laser characteristic, such as self-saturation and ANG, affects the photon number probability distribution. A good starting point is the four cases presented in the last section, where two modes have equal intensity, giving the strongest mode partition.

All multi-mode probability distribution results were simulated by using a time-step of 10 ps and over a period of 5 μs. Figure 10 depicts the simulated probability distributions for Case I. The total output gives a Gaussian distribution, while the modal distributions are dramatically different. The two dominant modes (11 and 12) exhibit quasi-uniform distributions compared to exponential distributions for modes 10 and 13.

Figure 11 shows simulated results for Case II. Interestingly, all probability distributions for the longitudinal modes shown exhibit a Gaussian shape similar to the total output. In Case II, self-saturation was simulated, allowing for the suppression of the dominant modes. It also meant that the relaxation oscillation dynamics would be dampened by this self-saturation factor. Comparison with Figure 10 suggests that the self-saturation factor has strong influence on the modal fluctuation or MPN.

Figure 12 shows results for Case III, while Figure 13 represents Case IV. These results are similar to Figure 10 and 11, respectively. As the laser parameters listed in Table 1-2 were extracted from the laser devices used by Ogita *et al.* [8], the simulated probability distributions shown in Figure 13 agree with the small fluctuations observed by Ogita *et al.* [8] in the mode-resolved transient measurements.

It can be concluded that ANG has a weak influence on the mode partition noise. However, it must be noted that the ANG strongly influences the spectral properties of semiconductor lasers. Results shown in Figures 12 and 13 once again support the claim earlier that MPN can be strongly influence by the self-saturation factor.

Of course, MPN would be influenced by other laser parameters such as differential gain, cavity and mirror losses and active volume dimensions etc. However, these parameters would also alter the threshold condition of the laser model. Marcuse [9-10] had studied the influence on MPN due to such parameters previously, so there is no need to repeat such simulations.

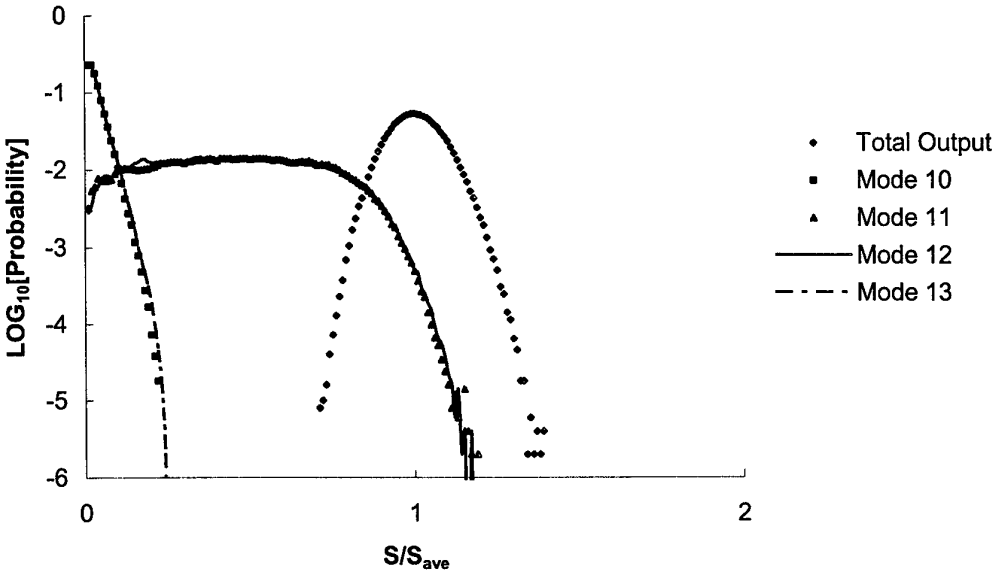

Figure 10: Photon number probability distribution as simulated from a noise-driven multi-mode rate-equation model with bias current of 20 mA, B_c=0, H_c=0 and $\Delta\lambda_{gp}$=+0.418 nm. The plot is normalised with the total average photon number.

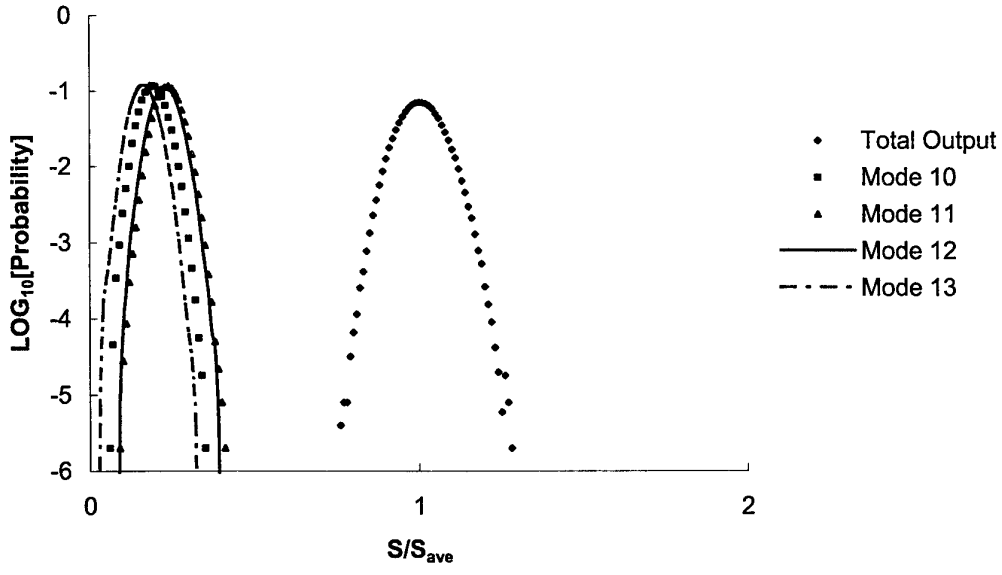

Figure 11: Photon number probability distribution as simulated from a noise-driven multi-mode rate-equation model with bias current of 20 mA, B_c=2x10^{-20} m^{3}s^{-1}, H_c=0 and $\Delta\lambda_{gp}$ =+0.418 nm. The plot is normalised with the total average photon number.

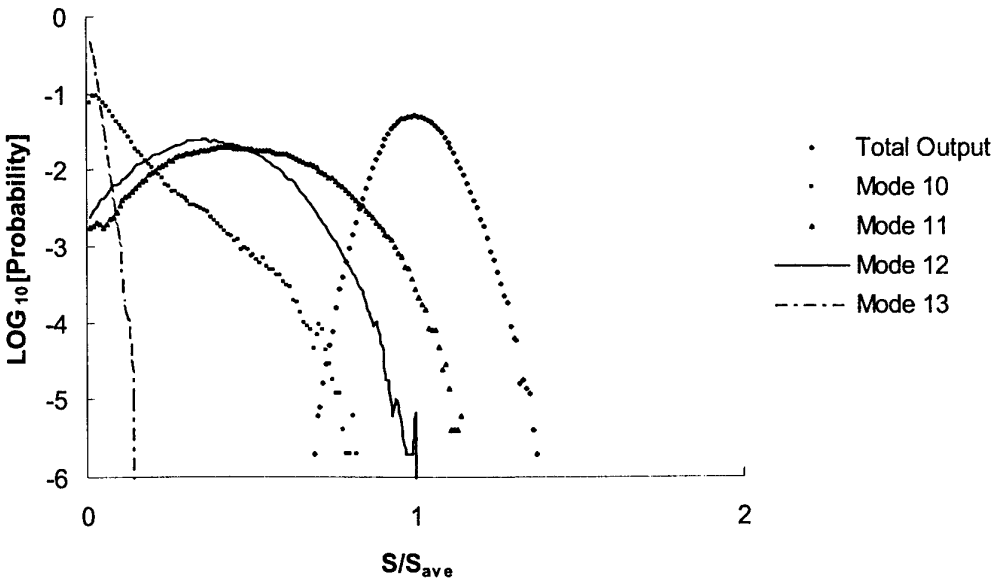

Figure 12: Photon number probability distribution as simulated from a noise-driven multi-mode rate-equation model with bias current of 20 mA, B_c=0, H_c=8x10^{-9} m^{3}s^{-2} and $\Delta\lambda_{gp}$=-0.465 nm. The plot is normalised with the total average photon number.

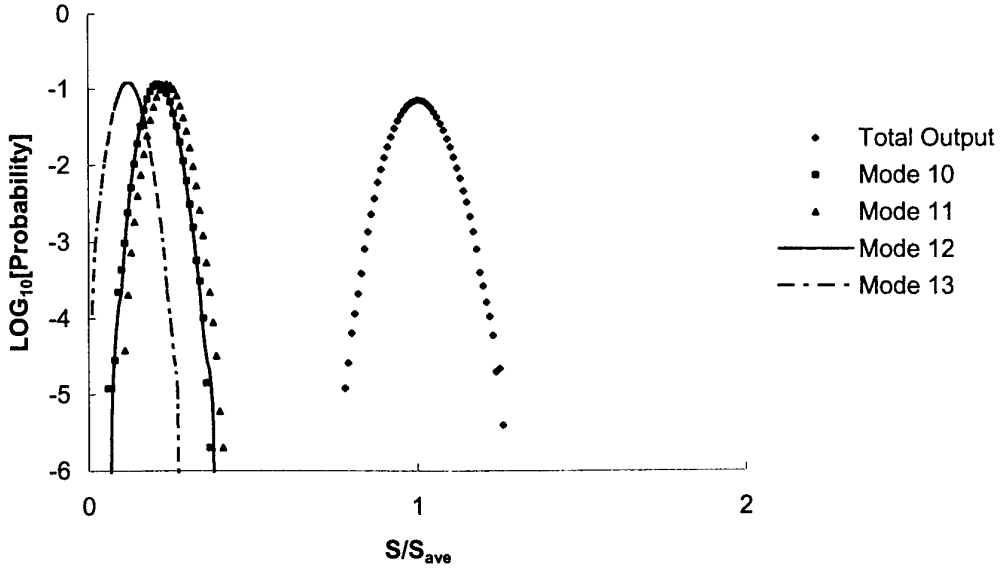

Figure 13: Photon number probability distribution as simulated from a noise-driven multi-mode rate-equation model with bias current of 20 mA, B_c=2x10^{-20} m^{3}s^{-1}, H_c=8x10^{-9} m^{3}s^{-2} and $\Delta\lambda_{gp}$=-0.150 nm. The plot is normalised with the total average photon number.

Recall the result presented earlier in Figure 5, which showed the influence of self-saturation on the probability distribution in the single-mode laser model, i.e. an increase in self-saturation would narrow the width of the probability distribution. The main conclusion put forward then was that the self-saturation factor dampens the relaxation oscillation interaction between the photon and carrier populations. This explanation is also applicable to the multi-mode results represented in Figures 11 and 13 when self-saturation was simulated. There is an added complexity in the multi-mode model compared to the single-mode case, which is the competition for available carriers between the longitudinal optical modes. The relaxation oscillation interaction is therefore not just between the total photon and carrier populations, but including the modal photon populations as well. So when self-saturation is simulated, it not only dampens the interaction between the total photon and carrier populations, but it also dampens the partition between the longitudinal optical modes, leading to Gaussian modal probability distributions. This phenomenon is clearly simulated and illustrated in Figures 10 and 11.

Case I (Figure 10) is interesting because the two dominant modes have quasi-uniform distributions and all the side modes have exponential distributions, while the total output distribution exhibits a Gaussian shape. This is the Central Limit Theorem at work. It would be of further interest to investigate how the shape of the probability distribution varies if a filter (e.g. a fibre Bragg grating) is applied to the total output. Table 3 lists two hypothetical optical bandpass filters to be applied to the total output in Case I.

	Mode 10	**Mode 11**	**Mode 12**	**Mode 13**
Filter 1	0.01	0.1	0.9	0.05
Filter 2	0.01	0.5	0.9	0.05

Table 3: Hypothetical filters to investigate the noise probability distribution for Case I.

Figure 14 depicts the probability distributions when both filters in Table 3 were applied and compared with the distribution of the total output, i.e. all-pass filter. Even in this Case 1 where the two dominant modes have quasi-uniform probability distributions, it takes only half of mode 11 being added to mode 12 to turn the distribution into a Gaussian shape as shown in Figure 14.

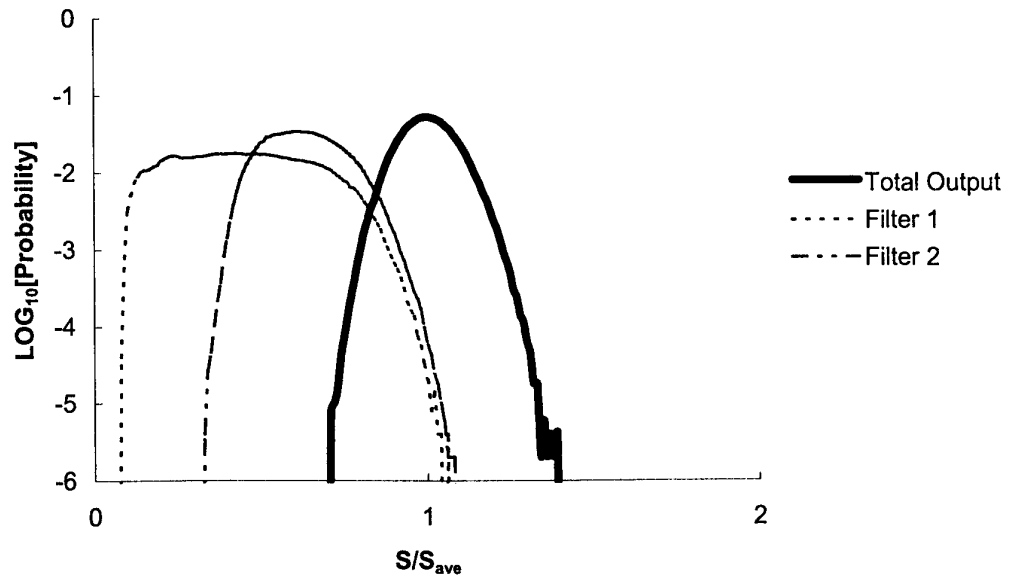

Figure 14: Photon number probability distribution as simulated for Case I and with filters applied to the output. The plot is normalised with the total average photon number.

In order to obtain two lasing modes in Case I, the gain peak was shifted positively, i.e. towards long-wavelength side, by 0.418 nm giving the quasi-uniform distributions seen in Figure 10. Note that this is half the mode spacing of the laser model. It is also worthwhile exploring the evolution of the probability distributions of modes 11 and 12 in Case I as the gain peak is shifted from 0.0 nm to 0.418 nm. The evolution of the probability distributions of modes 11 and 12 in Case I are illustrated in Figures 15 and 16, respectively. As the gain peak is shifted from 0.0 nm to 0.418 in the multi-mode model, the laser goes from having only one dominant mode to two dominant modes. As observed, mode 11 goes from having a Gaussian probability distribution to a quasi-uniform distribution, whereas mode 12 goes from exponential to quasi-uniform. If the gain peak were shifted positively to twice 0.418 nm, then mode 12 would be dominant over mode 11. Therefore, mode 12 would have a Gaussian distribution and mode 11 would be forced to become exponential. Liu *et al.* [1] experimentally observed modal probability distributions similar to those illustrated in Figures 15 and 16, suggesting that the laser device used in their experiment has very low self-saturation.

Since the modal probability distributions in Cases II and IV are Gaussian and those in Case III are Gaussian-like, the evolution of the modal probability distributions would be from Gaussian to Gaussian as the gain peak is shifted; unlike Case I, there would be very little information revealed from investigating these three cases. High level of self-saturation in multi-mode laser devices guarantees that modal probability distributions would be Gaussian regardless of where the material gain peak is located in relation to the FP laser cavity modes.

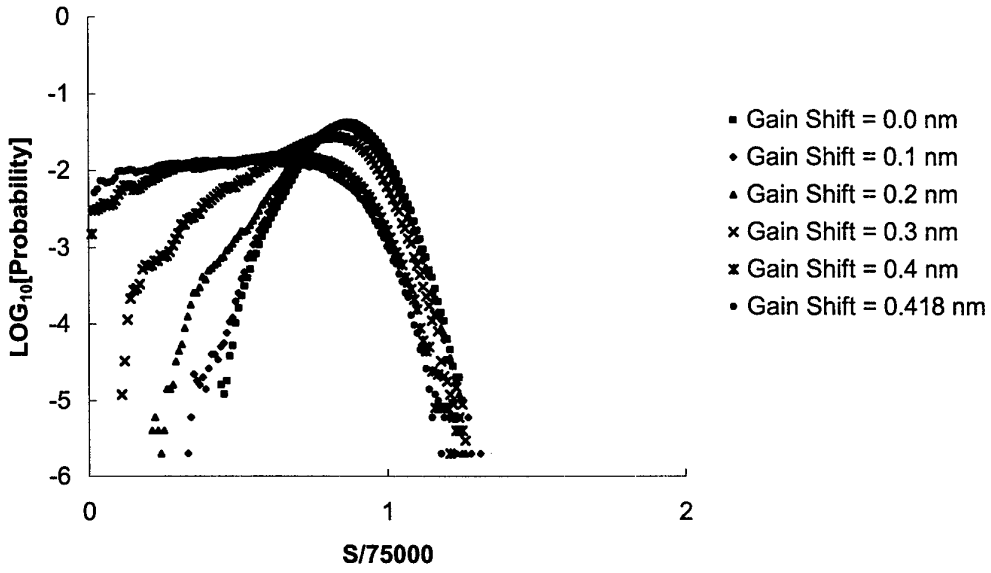

Figure 15: Evolution of the probability distribution of mode 11 as simulated for Case I. The plot is normalised with a common photon number of 75,000.

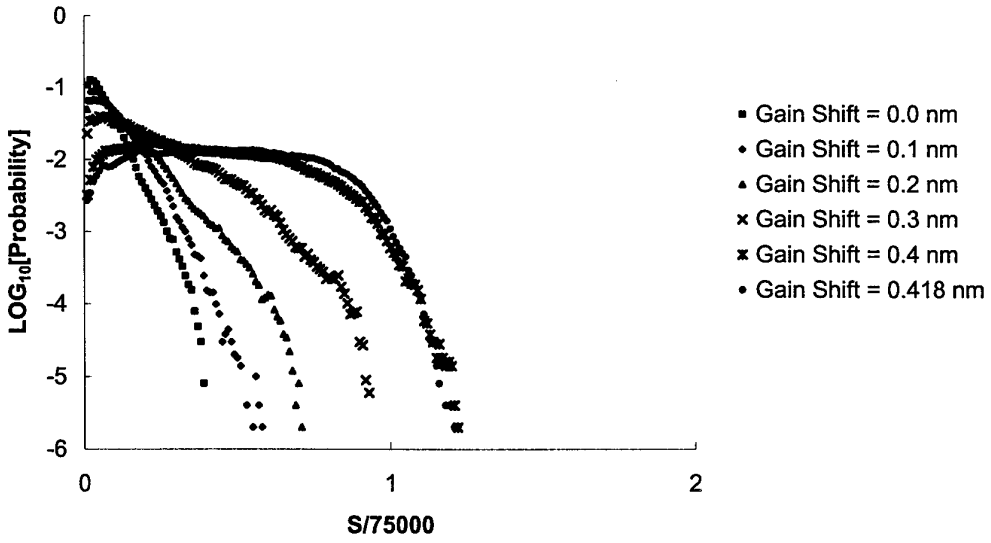

Figure 16: Evolution of the probability distribution of mode 12 as simulated for Case I. The plot is normalised with a common photon number of 75,000.

3.5 Single-Mode Results with Random Injection Current

Numerical investigation of MPN in semiconductor lasers would not be complete if the effect of injection current noise were not studied. It is expected that the current noise would be modulated onto the output photon number in some manner. Instead of using Equation 36, which gives a DC current at steady state, the following random current model was implemented to investigate the effect of current noise on mode partition:

$$I = I_{DC}(1+\sigma x_i) \tag{37}$$

where σ is the half-width of the overall current distribution and the random variable, x_i, is defined below for both uniform and Gaussian current distributions, respectively, using a random variable having a uniform distribution, $0 \le u \le 1$:

$$\begin{aligned} &\text{Uniform} \quad x_i = 2(u-0.5) \\ &\text{Gaussian} \quad x_i = \pm\sqrt{2}\,\text{erf}^{-1}(u) \end{aligned} \tag{38}$$

In all the following single-mode simulations, the half-width of the overall current distribution was arbitrarily chosen to be 20% of the average value. Figure 17 shows the results from the single-mode model when a uniform random injection current was used. Both deterministic and noise-driven models were simulated using the same current distribution. Also overlaid for reference is the probability distribution from Figure 3 when a DC current was used.

Interestingly, both the deterministic and noise-driven models gave Gaussian probability distributions for the output photon numbers. This illustrates that the observed Gaussian probability distributions in Figures 3-5 from earlier single-mode simulations were not due to the Gaussian noise models driving the rate equations, Equations 14-15, but were caused by the relaxation oscillation dynamics of the single-mode rate equations. The results in Figure 17 confirm the conclusion of the strong relationship between relaxation oscillation and MPN. Figure 18 shows results for a Gaussian current distribution, which again exhibit Gaussian probability distributions. However, the widths of the distributions in Figure 18 are wider, due to the large spread of the Gaussian tails in the injection current distribution.

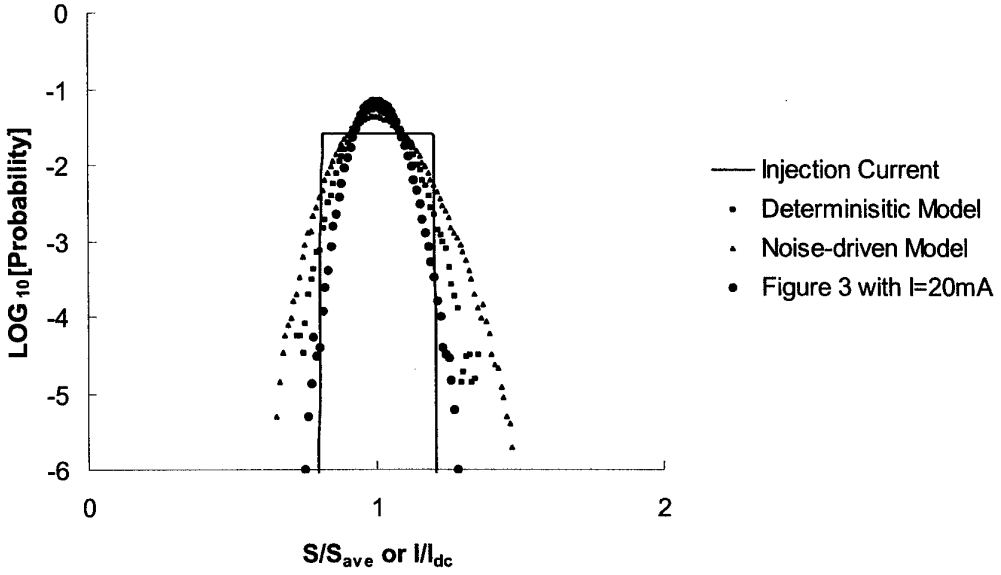

Figure 17: Photon number probability distribution from the single-mode model due to uniform random injection current. The plot is normalised with respective average value.

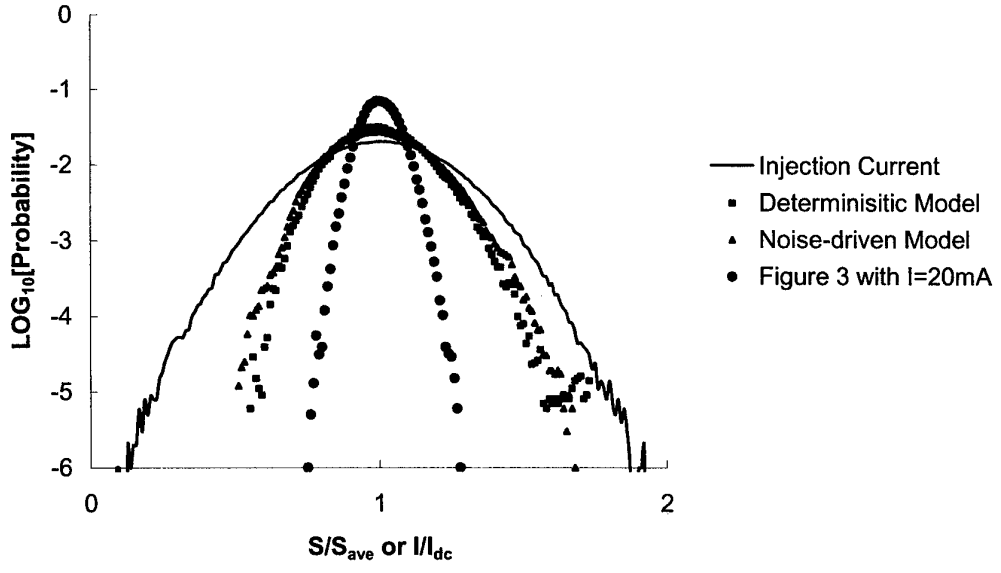

Figure 18: Photon number probability distribution from the single-mode model due to Gaussian random injection current. The plot is normalised with respective average value.

3.6 Multi-Mode Results with Random Injection Current

Similar to the results simulated using the single-mode laser models presented in the last section, the multi-mode laser models were injected with a uniform current distribution having a half-width equals to 20% of the average (DC) current. Initially, no self-saturation and asymmetric nonlinear gain were simulated, as in Figure 10. Other simulation parameters were set to the same values used in previous multi-mode simulations. The resultant probability distributions from the deterministic model are depicted in Figure 19.

In comparison to Figure 10, the modal probability distributions in Figure 19 are Gaussian. The explanation for this observation in Figure 19 can be derived from exploring the time-series outputs of the modal photon numbers of modes 11 and 12, which are the dominant contributors to the total output. The fluctuations from modes 11 and 12 in this case are in-phase with each other. On the contrary, Figure 10 shows two quasi-uniform modal probability distributions adding to give a resultant Gaussian distribution. This is because the modal fluctuations in Figure 10 were out of phase with each other. It is a very important observation.

Unlike the results from the single-mode laser models shown in Figures 17 and 18, Figure 19, together with Figure 10, illustrates that the Gaussian noise models in the multi-mode rate equations, Equations 23-24, are critical for simulating the correct MPN in multi-mode Fabry-Perot semiconductor lasers. Those Gaussian noise models allow the correct competition, both magnitude and phase properties, for the common carrier population to be simulated.

It is worth noting that the results observed here confirm that the deterministic multi-mode rate-equation laser model is accurate enough only to predict steady-state carrier and photon populations. It is not sufficient to simulate mode-partition dynamics in multi-mode Fabry-Perot semiconductor lasers. The noise-driven rate-equation laser model must be used.

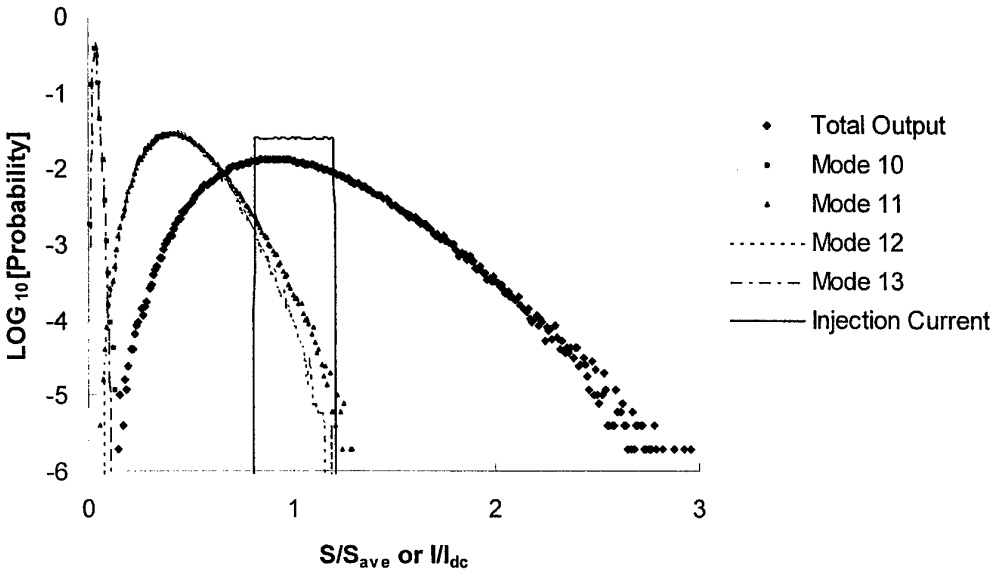

Figure 19: Photon number probability distribution from the deterministic multi-mode laser model without self-saturation and asymmetric nonlinear gain, due to a uniform injection current distribution. Photon number and current plot are normalised with their respective average values.

Figure 20 shows the same simulation using the noise-driven multi-mode laser model. The probability distribution of the total output is similar to that in Figure 19. However, the modal distributions are markedly different than those in Figure 19. They resemble those in Figure 10, but the quasi-uniform distributions have been stretched out into exponential distributions, due to the random injection current. The out-of-phase modal fluctuations between mode 11 and 12 were observed by inspecting the time-series outputs.

A similar simulation with self-saturation produced the results shown in Figure 21. The modal distributions replicate those in Figure 11. The distribution of the total output has been broadened due to the random injection current, but not as much as shown in Figure 20. The damping of the relaxation oscillation dynamics, caused by self-saturation, still influences how the modal and total power fluctuates even under noisy injection current.

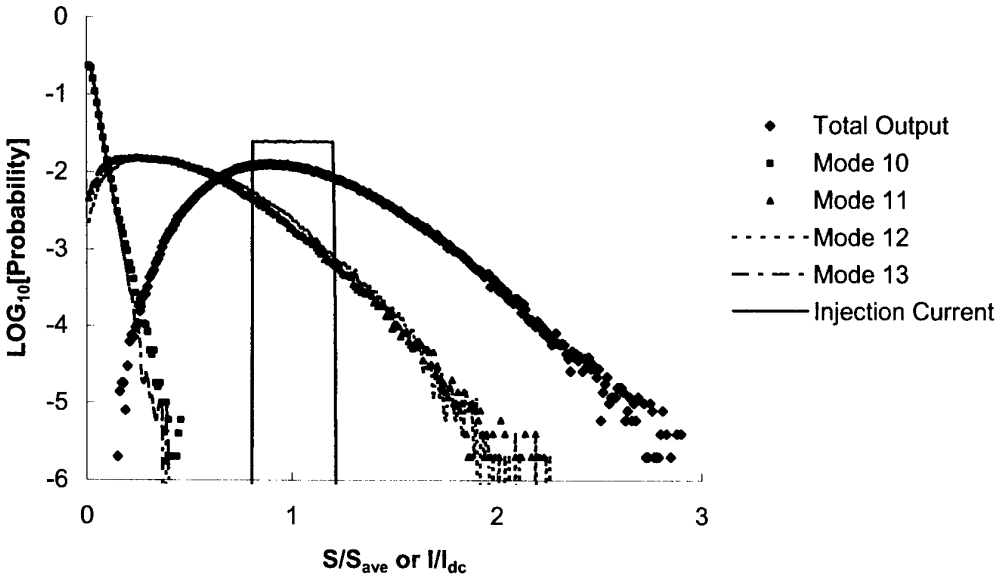

Figure 20: Probability distribution from the noise-driven multi-mode laser model without self-saturation and asymmetric nonlinear gain, due to a uniform injection current distribution. Photon number and current plot are normalised with their respective average value.

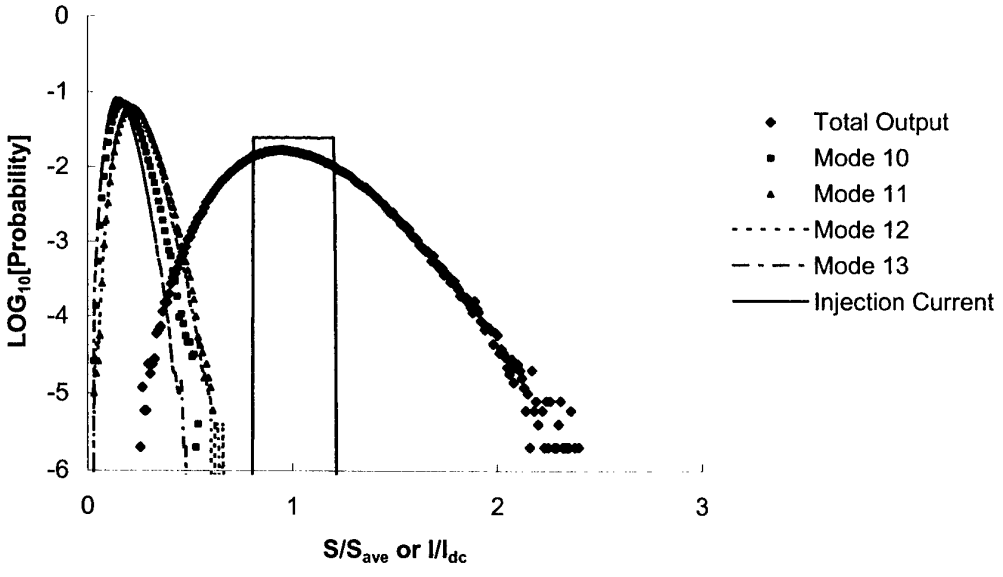

Figure 21: Probability distribution from the noise-driven multi-mode laser model with self-saturation, due to a uniform injection current distribution. Photon number and current plot are normalised with their respective average value.

3.7 Summary of Modelling Results

The main conclusions derived from the simulation results are:

1. Dynamics of relaxation oscillation influence the fluctuation of photon number in single-mode laser devices after the turn-on transient ceases.
2. Self-saturation dampens relaxation oscillation and thereby reduces fluctuation of photon number in single-mode laser devices.
3. Self-saturation strongly influences mode partitioning in multi-mode FP laser devices.
4. Asymmetric nonlinear gain alters distribution of longitudinal modes, but its effect on mode partitioning in FP devices is weaker than that of self-saturation.
5. High level of self-saturation in multi-mode laser devices guarantees that modal probability distributions would be Gaussian regardless of where the material gain peak is located in relation to the FP laser cavity modes.

High level of self-saturation reduces direct modulation bandwidth in semiconductor lasers. This has no direct consequence in microwave photonic signal processing when external modulation is used.

4. Experimental Investigation

4.1 Laser Characteristics

The experimental investigation into mode-partition noise was carried out using an Anritsu 5A211P2 (S/N: D05317) Fabry-Perot laser module. Its light-current characteristic is depicted below:

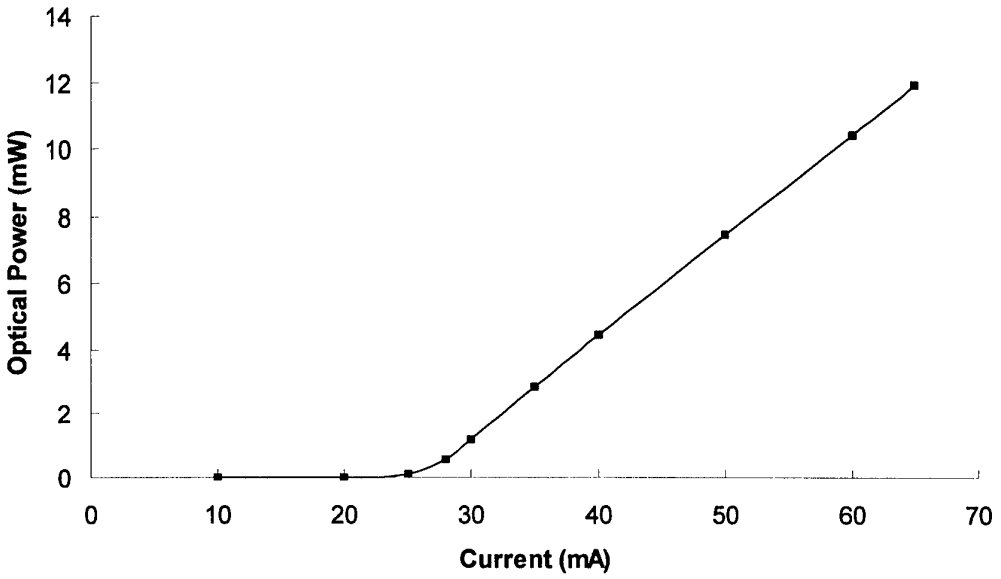

Figure 22: Light-current characteristic of the Anritsu 5A211P2 (S/N: D05317) Fabry-Perot semiconductor laser module.

The Anritsu MA9712A optical power sensor limits the maximum optical power reading on the curve. The supplier's test data indicates that the laser module is capable of emitting 150 mW of fibre output power at 700 mA. Figure 22 shows a threshold current of 26 mA. The optical spectra of the laser module for various bias currents are shown in Figure 23. These measurement and the rest of the experimental results presented in this section were obtained at the Photonics Research Laboratory, University of Melbourne. The evolution of the optical spectra as a function of the bias current suggests that the laser is a multiple quantum-well device. The asymmetricity of the optical spectra, together with multiple peaks indicates that the device is lasing from multiple quantised energy levels at high bias current. It is difficult to extract parameters with good certainty to simulate this laser device because it operates at different quantised levels as a function of bias current. This is certainly not a standard telecommunication device in which the lasing occurs from the first quantised level.

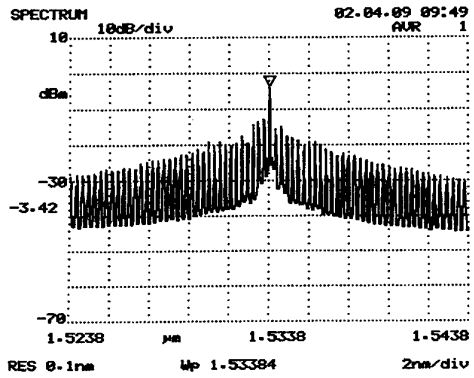

(a) Bias = 31 mA

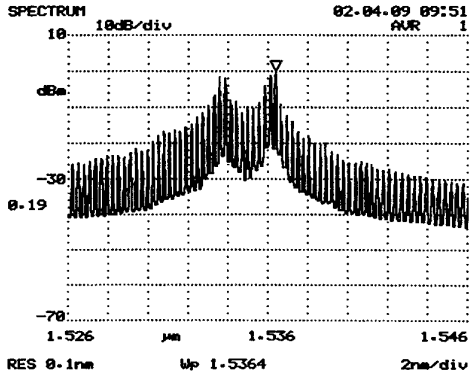

(b) Bias = 50 mA

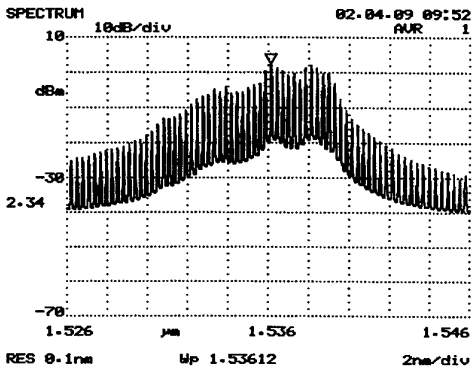

(c) Bias = 100 mA

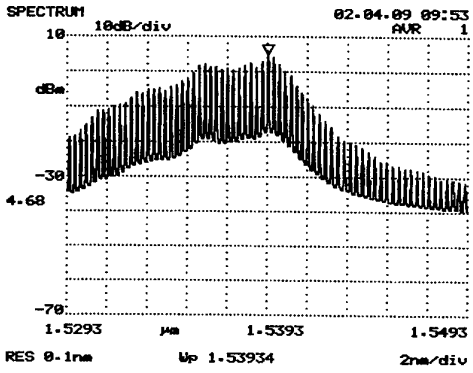

(d) Bias = 150 mA

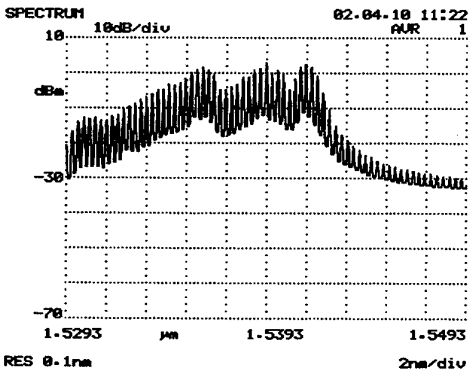

(e) Bias = 200 mA

Figure 23: Optical spectra of the Anritsu 5A211P2 (S/N: D05317) Fabry-Perot semiconductor laser module at various bias currents.

4.2 Relative-Intensity Noise

Figure 24 shows the RIN plots of the laser module at 150 mA. The first plot is the RIN spectrum without any optical filtering. An attenuation (HP 8156A) of 10 dB was used to reduce the input power to the HP 70000A RIN Analyser. It shows that the RIN is just above the thermal noise limit of the analyser, and the relaxation oscillation of the laser at 150 mA peaks at approximately 7 GHz. This relaxation oscillation peak is weak, indicating a high damping characteristic. The strength of this relaxation oscillation of this laser module did not change significantly with bias current.

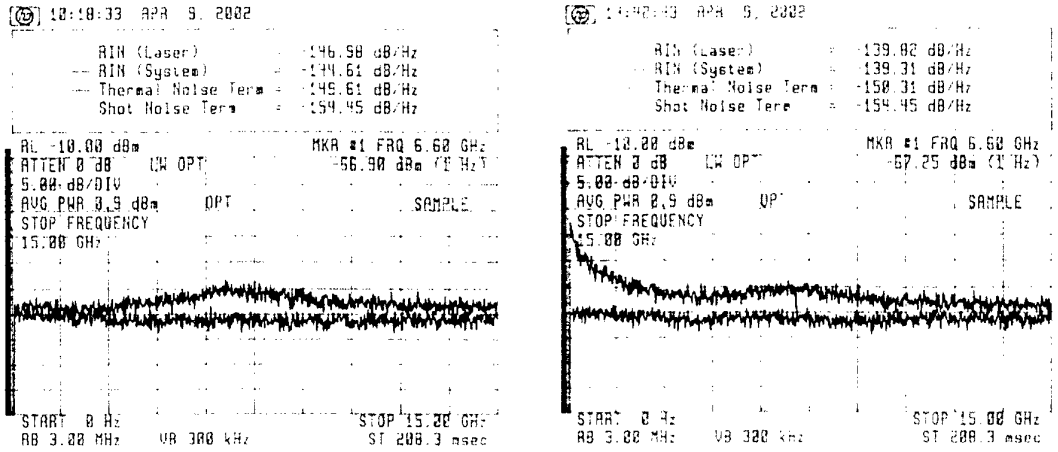

(a) No filter *(b) With bandpass filter*

Figure 24: Typical RIN spectra of the Anritsu 5A211P2 (S/N: D05317) semiconductor laser module at 150 mA. Also shown are the thermal noise spectra (flat) as measured using the Hewlett-Packard 70000A RIN analyser.

The output of the laser module was then passed through a JDS Fitel TB1570 bandpass filter. The filter was tuned to the peak of the optical spectrum shown in Figure 23(d). An attenuation of 7 dB was required in this case. The RIN spectrum is shown as the second plot of Figure 24. As expected, it shows an increase in RIN at low frequencies [13]. This enhancement of the low-frequency RIN is due mainly to the mode-partition noise of the dominant longitudinal modes, which passed through the bandpass filter.

4.3 Noise Power Probability Distributions

To observe the intensity noise power probability distribution, a Tektronix CSA 803 was used. The optical output was input into a New Focus 45 GHz detector, whose output was then fed into a Tektronix SD-30 sampling head. A detector having large bandwidth was used to ensure that noise fluctuations at high frequencies were also detected and not averaged out. The histogram of the fluctuations, in logarithmic scale, then provides the probability distribution of the intensity noise.

Figure 25 illustrates the intensity noise power distribution of the laser output at bias currents of 31, 50, 100 and 150 mA. A minimum of one million samples was used to obtain the histograms. The four histograms in Figure 25 depict a Gaussian distribution. The increase in the average voltage is due to the increase in laser output as a function of bias current. Interestingly, all the histograms are the same. This is consistent with the simulated result shown in Figure 4 earlier, which depicted that the magnitude of intensity noise fluctuation remains the same above threshold.

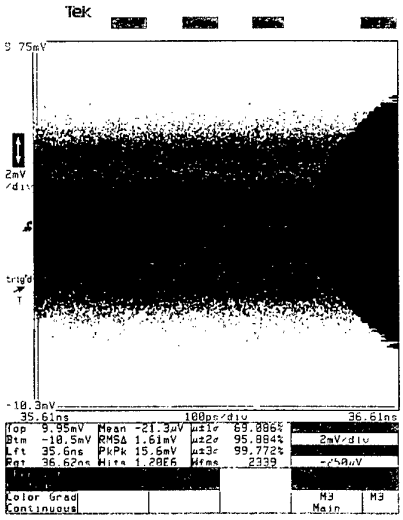

(a) Bias=31 mA

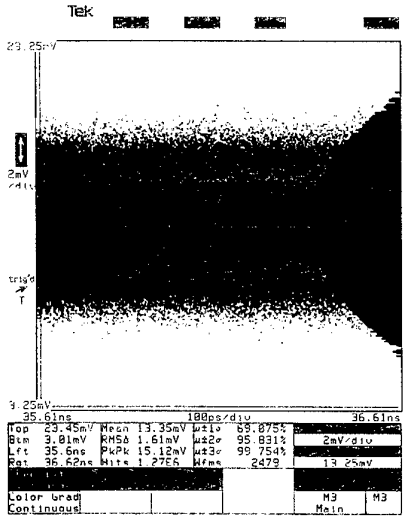

(b) Bias=50 mA

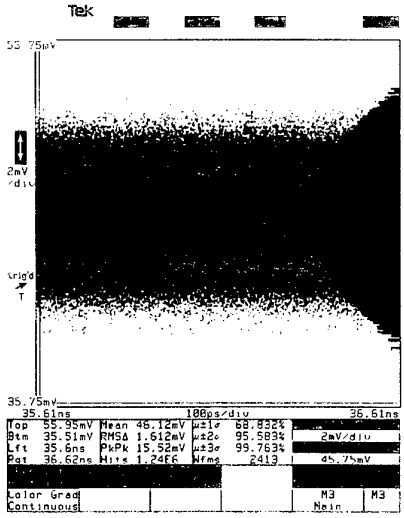

(c) Bias=100 mA

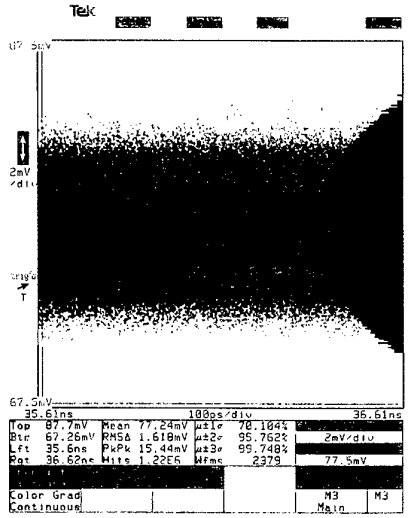

(d) Bias=150 mA

Figure 25: Intensity noise power distribution of the laser's CW output at various bias currents. The laser's output was not spectrally modified with filters of any form.

Figure 26 shows the intensity noise distribution of the filtered output of the laser module at 150 mA. The filter used was a JDS Fitel TB1570 filter. The optical spectrum shown in Figure 26(a) is also applicable to RIN spectrum shown in Figure 24(b). The magnitude of the intensity noise fluctuation shown in Figure 26 is larger than that depicted in Figure 25. This is consistent with the observation of low-frequency RIN enhancement in Figure 24.

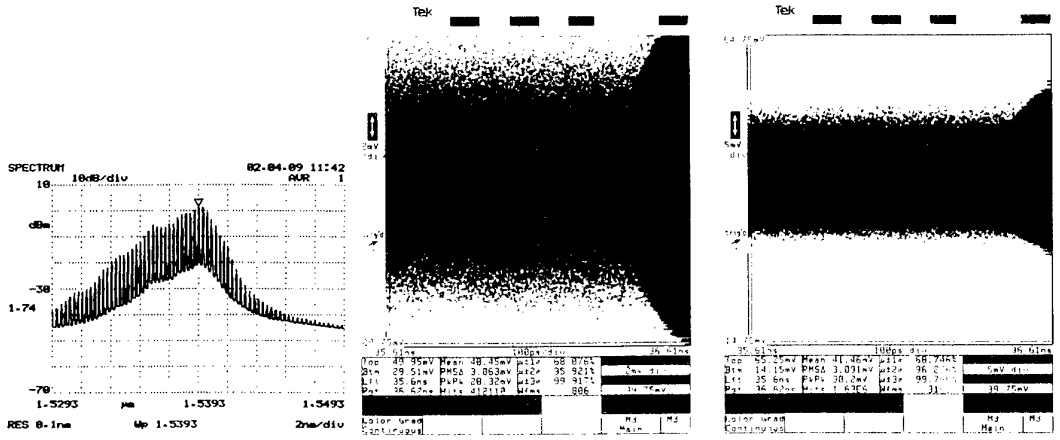

(a) Filter centred at peak of the spectrum at 150 mA

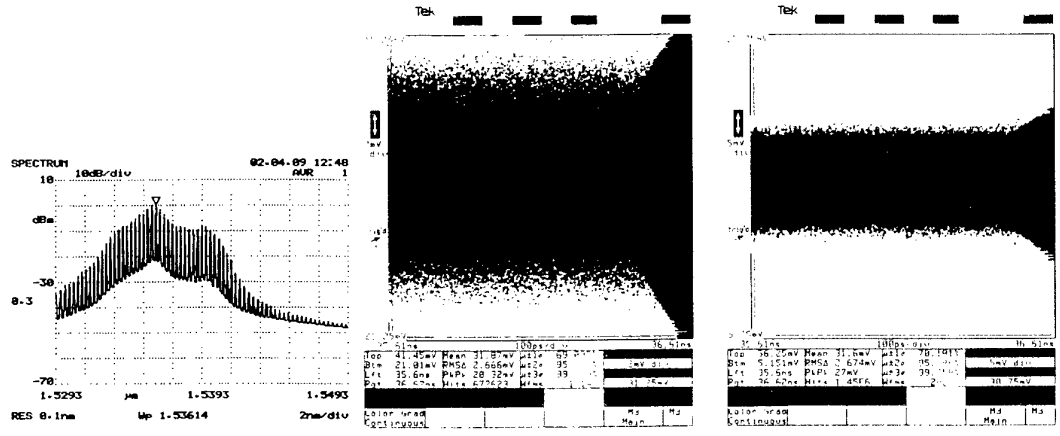

(b) Filter centred on the low-wavelength side of the spectrum at 150 mA

Figure 26: Intensity noise power distribution of filtered laser output at 150 mA. The histograms were plotted using two scales of 2mV/div and 5mV/div, respectively, for clarity.

The results depicted in Figure 26 are again Gaussian as there are still many longitudinal modes able to pass through the relatively large passband of the filter. However, the important impact is the larger magnitude of the fluctuation.

More measurements were performed by passing the laser output through a NEL 4x4 arrayed-waveguide grating multiplexer (AWGM) and JDS Uniphase 1532-nm fibre Bragg grating (FBG). There was no FBG available closer to the peak of the optical spectrum around 1540 nm available at the time these measurements were taken. The reflection from the FBG was extracted by using a Photonic Technology Halo optical circulator. When the filtered output was input into the New Focus detector, the optical power level was actually below its sensitivity and so it registered zero reading even when the bias current was increased from 150 mA to 200 mA. A more suitable detector comes in the form of the 22 GHz lightwave section (HP 70810B) of the RIN analyser. This detector provides a RF output without any DC component. So the fluctuation from this detector would always be centred at 0V, unlike that of the New Focus detector. Figure 27 shows measurements from the output 1 of the AWGM. The optical spectrum clearly depicts the free spectral range of the AWGM. The results from output 1 are indicative of other output ports.

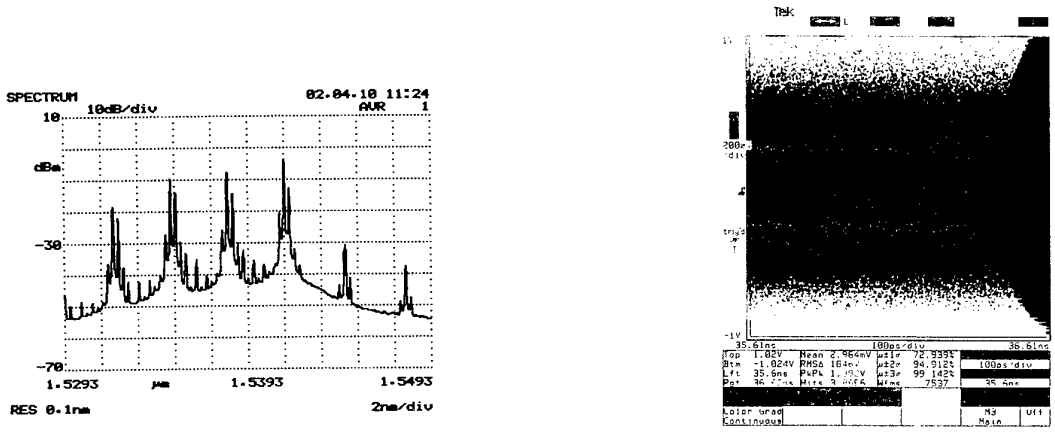

Figure 27: Intensity noise power distribution of laser output biased at 200 mA passing through a 4x4 AWGM.

Figure 28 shows measurements from the FBG. The distribution of the intensity noise shown in Figure 27 is not perfectly Gaussian, but it is still symmetric. However, the distribution shown in Figure 28 is clearly asymmetric and cannot be concluded as a perfect Gaussian shape. Be aware of the different mV/div scales used in Figures 27 and 28. The asymmetry observed, which is more obvious in the logarithmic plot compared to the linear version, is likely to be the uncorrelation of all the longitudinal modes [9] and its clarity was mainly due to a smaller mV/div scale used.

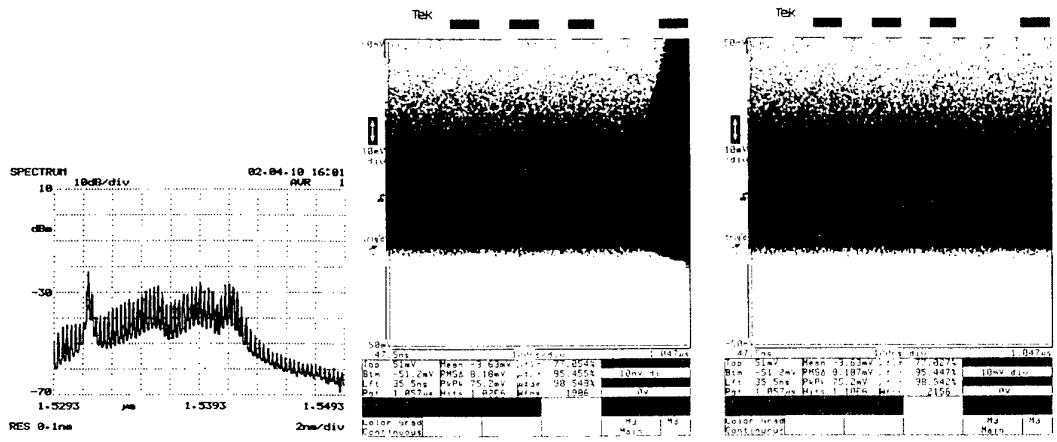

Figure 28: Intensity noise power distribution of laser output at 200 mA reflected from a fibre Bragg grating as extracted from an optical circulator. The histograms were plotted for both logarithmic and linear scales, respectively.

If a FBG was centred near the peak of the spectrum around 1540 nm, it is believed that the noise power distribution would still be Gaussian-like, as indicated by the results when a bandpass filter (Figure 26) and AWGM (Figure 27) were used. The main reason is that multiple modes would still be reflected from the FBG.

In order to be conclusive with the noise distribution measurements of each mode presented in this section, a narrow monochromator is required to filter out each longitudinal mode without the presence of other modes on both sides.

Nevertheless, it can be seen from the measurements presented in this section, together with the simulation results, that multi-mode FP laser devices do have applications in DWDM microwave photonic signal processing. However, there are many issues that must be considered:

1. Self-saturation level present in the laser device.
2. Utilising FP modes around the peak of the optical spectrum only to have the highest likelihood of gaining symmetric intensity noise distribution, unlike that shown in Figure 28.
3. Using optical filters, such as FBG, to pick out at least a couple of modes, per channel, together they would provide an intensity noise distribution that is Gaussian.
4. Issues 2 & 3 would place a limit on the number of DWDM channels available from FP laser devices as multi-wavelength sources.

5. Conclusions

The conclusions derived from the simulation results of multi-mode FP semiconductor lasers are:

1. Self-saturation strongly influences mode partitioning in multi-mode FP laser devices.
2. Asymmetric nonlinear gain alters distribution of longitudinal modes, but its effect on mode partitioning in FP devices is weaker than that of self-saturation.
3. High level of self-saturation in multi-mode laser devices guarantees that modal probability distributions would be Gaussian regardless of where the material gain peak is located in relation to the FP laser cavity modes.

These simulation results were also able to illustrate both reported observations by Ogita *et al.* [8] and Liu *et al.* [1]. The linkage between the simulations and the reported observations is believed to be the self-saturation or gain compression factor due to non-linearities in semiconductor lasers. The simulations presented here were based on rate equations and laser parameters from Ogita *et al.* [8]. When self-saturation was simulated, it produced Gaussian modal probability distributions as expected from the mode-resolved power transients reported in Ogita *et al.* [8]. However, simulations without self-saturation produced modal fluctuation from zero to the average total power, which has been classed as quasi-uniform distributions. This supports the observations by Liu *et al.* [1], indicating that the lasers used in that work had very low self-saturation.

The influence of self-saturation on mode-partition noise is the major finding presented in this report. This finding is independently supported by a newly published research paper concluding that mode competition in semiconductor lasers is caused by nonlinear gain saturation effects [20].

Experimentally, power fluctuation measurements were carried out using a high-power 1550-nm Fabry-Perot semiconductor laser. Experimental evidence indicates that the modal probability distribution is Gaussian. The laser device available operates in different regimes as a function of injected current, which makes it difficult to extract parameters with good certainty to simulate the device. In order to be conclusive with the noise distribution measurements of each mode, a narrow monochromator would be required to filter out each longitudinal mode without the presence of other modes on both sides.

Based on simulation results presented in this report, together with basic measurements from a high-power Fabry-Perot laser device, it can be concluded that multi-mode Fabry-Perot having high self-saturation would produce Gaussian modal fluctuations or MPN. Such device may be a candidate as multi-wavelength source in microwave photonic signal processing for ES applications, in which a wavelength-division

multiplexing technique is employed. However, the number of DWDM channels available from these FP laser devices would be limited depending on their optical spectra.

6. Recommendations

Multi-mode FP laser devices can be utilised in DWDM microwave photonic signal processing. However, the following issues must be considered.

1. It would only be suitable for applications where the number of DWDM channels required is low.
2. Only select FP laser devices that have high level of self-saturation.
3. Only utilise FP modes around the peak of the optical spectrum.
4. Use optical filters, such as FBG, to pick out at least a couple of modes per channel.

Recommended future directions to complement the research presented in this report are:

1. Investigating techniques to destroy coherence in DFB laser devices because they would allow a high number of DWDM channels to be used in microwave photonic signal processor.
2. Investigating erbium-doped fibre (EDF) ring laser configuration as an incoherent multi-wavelength source suitable for DWDM microwave photonic signal processing.

Understanding these two laser technologies, as well as FP laser devices, would provide engineers with alternative design solutions in the development of photonic EW systems.

7. References

[1] P-L.Liu and K.Ogawa, "Statistical measurement as a way to study mode partition in injection laser", *IEEE Journal of Lightwave Technology*, **2**, pp. 44-48, 1984

[2] C.H.Henry, P.S.Henry and M.Lax, "Partition fluctuation in nearly single-longitudinal-mode lasers", *IEEE Journal of Lightwave Technology*, **2**, pp. 209-216, 1984

[3] E.E.Basch, R.F.Kearns and T.G.Brown, "The influence of mode partition on nearly single longitudinal mode lasers", *IEEE Journal of Lightwave Technology*, **4**, pp. 516-516, 1986

[4] K.Ogawa and R.S.Vodhanel, "Measurements of mode partition noise of laser diodes", *IEEE Journal of Quantum Electronics*, **18**, pp. 1090-1093, 1982

[5] P-L.Liu and M.M.Choy, "Effect of bias on transient mode partition – An analysis based on photon statistics", *IEEE Journal of Quantum Electronics*, **25**, pp. 854-857, 1989

[6] M.Ohtsu and Y.Teramachi, "Analyses of mode partition and mode hopping in semiconductor lasers", *IEEE Journal of Quantum Electronics*, **25**, pp. 31-38, 1989

[7] A.Valle, C.R.Mirasso and L.Pesquera, "Mode partition noise of nearly single-mode semiconductor lasers modulated at GHz rates", *IEEE Journal of Quantum Electronics*, **31**, pp. 876-885, 1995

[8] S.Ogita, A.J.Lowery and R.S.Tucker, "Influence of asymmetric nonlinear gain on the transient intensities of longitudinal modes in long wavelength Fabry-Perot laser diodes", *IEEE Journal of Quantum Electronics*, **33**, pp. 198-210, 1997

[9] D.Marcuse, "Computer simulation of laser photon fluctuations: Theory of single-cavity laser", *IEEE Journal of Quantum Electronics*, **20**, pp. 1139-1148, 1984

[10] D.Marcuse, "Computer simulation of laser photon fluctuations: Single-cavity laser results", *IEEE Journal of Quantum Electronics*, **20**, pp. 1148-1155, 1984

[11] D.Marcuse, "Computer simulation of laser photon fluctuations: Coupled-cavity lasers", *IEEE Journal of Quantum Electronics*, **21**, pp. 154-161, 1985

[12] D.Marcuse, "Computer simulation of laser photon fluctuations: DFB lasers", *IEEE Journal of Quantum Electronics*, **21**, pp. 161-167, 1985

[13] G.L.B.Loh, "Characterisation of relative intensity noise in semiconductor lasers", *Master Thesis at the University of Melbourne*, 1994

[14] D.Pastor, J.Capmany, S.Sales, P.Munoz and B.Ortega, "Reconfigurable fibre-optic-based RF filters using injection in multimode lasers", *IEEE Photonic Technology Letters*, **13**, pp. 1224-1226, 2001

[15] K.N.Park, Y.T.Lee, M.H.Kim, K.S.Lee and Y.H.Won, "All-fibre drop-pass filters with fibre Bragg gratings", *IEEE Photonic Technology Letters*, **10**, pp. 555-557, 1998

[16] D.Pastor, J.Capmany and B.Ortega, "Experimental demonstration of parallel fibre-optic-based RF filtering using WDM techniques", *IEEE Photonic Technology Letters*, **12**, pp. 77-78, 2000

[17] C.H.Henry, "Theory of the linewidth of semiconductor lasers", *IEEE Journal of Quantum Electronics*, **18**, pp. 259-264, 1982

[18] E.Kreyzig, "Advanced Engineering Mathematics", John Wiley & Sons

[19] G.P.Agrawal and N.K.Dutta, "Long-wavelength semiconductor lasers", Van Nostrand Reinhold

[20] M.Ahmed and M.Yamada, "Influence of instantaneous mode competition on the dynamics of semiconductor lasers", *IEEE Journal of Quantum Electronics*, **38**, pp. 682-693, 2002

DISTRIBUTION LIST

Mode-Partition Noise in Semiconductor Lasers

Linh V T Nguyen

AUSTRALIA

DEFENCE ORGANISATION

Task Sponsor - DGSPD

S&T Program

Chief Defence Scientist
FAS Science Policy
AS Science Corporate Management
Director General Science Policy Development
} shared copy

Counsellor Defence Science, London (Doc Data Sheet)
Counsellor Defence Science, Washington (Doc Data Sheet)
Scientific Adviser to MRDC Thailand (Doc Data Sheet)
Scientific Adviser Joint
Navy Scientific Adviser (Doc Data Sheet and distribution list only)
Scientific Adviser - Army (Doc Data Sheet and distribution list only)
Air Force Scientific Adviser
Director Trials

Systems Sciences Laboratory

Chief, Electronic Warfare & Radar Division	Doc Data Sheet
Research Leader, Electro-Optic Electronic Warfare	Doc Data Sheet
Head, EO Technology	Doc Data Sheet
Dr. David Hunter, EWRD	Doc Data Sheet
Dr. Tim Priest, EWRD	Doc Data Sheet
Dr. Kamal Gupta, EWRD	Doc Data Sheet
Linh V T Nguyen, EWRD	

DSTO Library and Archives

Library Edinburgh
Australian Archives
US Defense Technical Information Center, 2 copies
UK Defence Research Information Centre, 2 copies
Canada Defence Scientific Information Service
NZ Defence Information Centre

Capability Systems Staff

Director General Maritime Development (Doc Data Sheet only)
Director General Aerospace Development (Doc Data Sheet only)

Knowledge Staff

Director General Command, Control, Communications and Computers (DGC4)
(Doc Data Sheet only)

Army

ABCA National Standardisation Officer, Puckapunyal, 4 copies
SO (Science), Deployable Joint Force Headquarters (DJFHQ) (L), Enoggera QLD (Doc Data Sheet only)

Intelligence Program

DGSTA Defence Intelligence Organisation
Manager, Information Centre, Defence Intelligence Organisation

Corporate Support Program

Library Manager, DLS-Canberra
Library Manager, Defence Library Service - Sydney West (Doc Data Sheet only)

UNIVERSITIES AND COLLEGES

Australian Defence Force Academy
Library
Head of Aerospace and Mechanical Engineering
Serials Section (M list), Deakin University Library, Geelong, VIC
Hargrave Library, Monash University (Doc Data Sheet only)
Librarian, Flinders University

OTHER ORGANISATIONS

NASA (Canberra)
State Library of South Australia

OUTSIDE AUSTRALIA

ABSTRACTING AND INFORMATION ORGANISATIONS

Library, Chemical Abstracts Reference Service
Engineering Societies Library, US
Materials Information, Cambridge Scientific Abstracts, US
Documents Librarian, The Center for Research Libraries, US

INFORMATION EXCHANGE AGREEMENT PARTNERS

Acquisitions Unit, Science Reference and Information Service, UK
Library - Exchange Desk, National Institute of Standards and Technology, US

SPARES (5 copies)

Total number of copies: **38**

DEFENCE SCIENCE AND TECHNOLOGY ORGANISATION
DOCUMENT CONTROL DATA

1. PRIVACY MARKING/CAVEAT (OF DOCUMENT)
UNCLASSFIED

2. TITLE

Mode-partition Noise in Semiconductor Lasers

3. SECURITY CLASSIFICATION (FOR UNCLASSIFIED REPORTS THAT ARE LIMITED RELEASE USE (L) NEXT TO DOCUMENT CLASSIFICATION)

Document	(U)
Title	(U)
Abstract	(U)

4. AUTHOR(S)

Linh V. T. Nguyen

5. CORPORATE AUTHOR

Systems Sciences Laboratory
PO Box 1500
Edinburgh South Australia 5111 Australia

6a. DSTO NUMBER	6b. AR NUMBER	6c. TYPE OF REPORT	7. DOCUMENT DATE
DSTO-TR-0244	AR-012-452	Research Report	September 2002

8. FILE NUMBER	9. TASK NUMBER	10. TASK SPONSOR	11. NO. OF PAGES	12. NO. OF REFERENCES
E 9505-23-105 1	LRR 02/178	DGSPD	50	20

13. URL on Worldwide Web

http://www.dsto.defence.gov.au/corporate/reports/DSTO-RR-0244

14. RELEASE AUTHORITY

Chief, Electronic Warfare & Radar Division

15. SECONDARY RELEASE STATEMENT OF THIS DOCUMENT

Approved for Public Release

OVERSEAS ENQUIRIES OUTSIDE STATED LIMITATIONS SHOULD BE REFERRED THROUGH DOCUMENT EXCHANGE, PO BOX 1500, EDINBURGH, SA 5111

16. DELIBERATE ANNOUNCEMENT
No Limitations

17. CITATION IN OTHER DOCUMENTS Yes

18. DEFTEST DESCRIPTORS

Semiconductor lasers
Mode-partition noise (MPN)
Numerical simulation
Signal processing
Gaussian noise
Multiplexing
Noise
Noise measurement
Modelling
Relaxation oscillators
Noise spectra

19. ABSTRACT

The primary goal of this research activity is to understand a range of applicability of different types of lasers to a variety of electronic warfare (EW) applications. This work helps by providing a detailed understanding of mode-partition noise (MPN) in multi-mode Fabry-Perot (FP) semiconductor lasers. MPN in semiconductor lasers describes how the intensities of all longitudinal optical modes fluctuate as they compete with each other for a common injected-carrier population.

The results presented in this report include both numerical simulations and experimental measurements. The numerical simulations are based on a noise-driven 21-mode rate-equation laser model, which enables multiple mode partition to be modelled. The formulation of the laser model allows for variation of laser parameters to investigate their effect on mode-partition noise. To the author's best knowledge, only studies with variation of trivial laser parameters have been reported previously. The results in this report go beyond these existing studies in the literature.

Experimental measurements are used to verify simulations where possible. The main difficulty in this work is having laser devices with different parameters as in the simulations. In addition, the available laser device operates in different regimes as a function of injected current, making it difficult to extract parameters with good certainty to simulate the device.

SYSTEMS SCIENCES LABORATORY
PO BOX 1500 EDINBURGH SOUTH AUSTRALIA, 5111
AUSTRALIA, TELEPHONE (08) 8259 5555